Nano Research

Open Access

Review Article

Recent progress in intrinsic defect modulation of g-C_3N_4 based materials and their photocatalytic properties

Sichang Wang[1], Liting Wang[1], Wan Liu[2], Congyu Ke[1] ✉, Miao Li[1] ✉, and Junfeng Hui[2] ✉

[1] *College of Chemistry and Chemical Engineering, Xi'an Shiyou University, Xi'an 710065, China*
[2] *School of Chemical Engineering, Northwest University, Xi'an 710069, China*

Cite this article: *Nano Research*, **2025**, *18*, 94907125. https://doi.org/10.26599/NR.2025.94907125

ABSTRACT: The application of solar-driven photocatalytic processes shows considerable potential for renewable energy production and environmental remediation. Graphitic carbon nitride (g-C_3N_4) has emerged as a highly promising metal-free photocatalyst due to its outstanding electronic structure and physicochemical properties. However, the intrinsic constraints of pristine g-C_3N_4, such as limited visible light absorption range, high recombination rates of photogenerated charge carriers, and a scarcity of active sites, have significantly hindered its photocatalytic performance and practical implementations. Recent studies have demonstrated that defect engineering can substantially mitigate these issues by enhancing both light absorption and charge separation efficiency, thereby improving photocatalytic performance. This review provides a comprehensive overview of intrinsically defective g-C_3N_4-based materials, focusing on the types of intrinsic defects, their modification strategies, and the recent advancements in the field. It also highlights the diverse applications of defect-modified g-C_3N_4, including wastewater remediation, hydrogen evolution, CO_2 conversion, NO removal, nitrogen fixation, photocatalytic disinfection, and H_2O_2 production. Finally, the current challenges and future perspectives are discussed of g-C_3N_4-based photocatalytic materials, offering insights and practical guidance for the development of advanced g-C_3N_4-based photocatalysts.

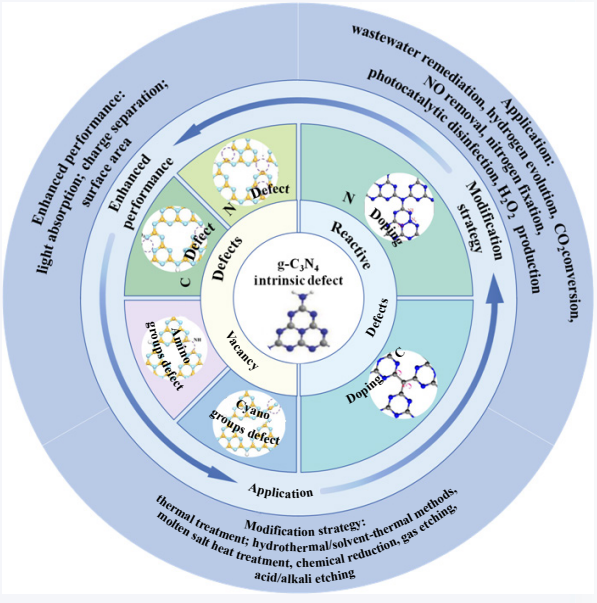

KEYWORDS: defect modulation, photocatalysis, graphitic phase carbon nitride, intrinsic defects

1 Introduction

With the rapid development of global industrialization, energy shortage and environmental pollution have become the most urgent problems for human development in the 21st century [1–3]. The reserves of conventional fossil fuels have been dwindling for an extended period, and their extraction and utilization pose irreversible consequences on the global ecosystem and surroundings. Consequently, the exploration of sustainable and clean energy alternatives including solar, wind, nuclear, and hydroelectric power holds great potential to effectively address the issues mentioned above. As the main energy source on the earth, solar energy can fully satisfy the total amount of energy that human beings need. However, solar energy is characterized by its instability and low energy density. Therefore, optimizing the conversion, storage, and utilization of solar energy is crucial in addressing the issue of energy scarcity. Photocatalytic technology can convert solar energy into the energy humans require at warm ambient temperatures and pressures. This technology is environmentally friendly cost-effective, and offers high selectivity [4–7]. As a result, photocatalytic technology is regarded as a promising solution to address the urgent issues of energy shortages and environmental pollution associated with fossil fuels.

Among a wide range of reported semiconductor photocatalytic

Received: September 29, 2024; **Revised:** November 7, 2024
Accepted: November 11, 2024

✉Address correspondence to Congyu Ke, kcy@xsyu.edu.cn; Miao Li, limiao2017@xsyu.edu.cn; Junfeng Hui, huijunfeng@nwu.edu.cn

materials, graphite carbon nitride (g-C_3N_4) is a two-dimensional (2D) carbon-nitride-based material with a layered structure similar to graphite. Triazine (Fig. 1(a)) and tri-s-triazine (Fig. 1(b)) are the primary constituent units of g-C_3N_4, which are formed through a π-conjugated structure with the C and N atoms sp^2-hybridization [8]. The g-C_3N_4 material exhibits advantages of high absorption capacity for visible light, low cost, excellent optical and electronic properties, tunability in composition and good thermal and

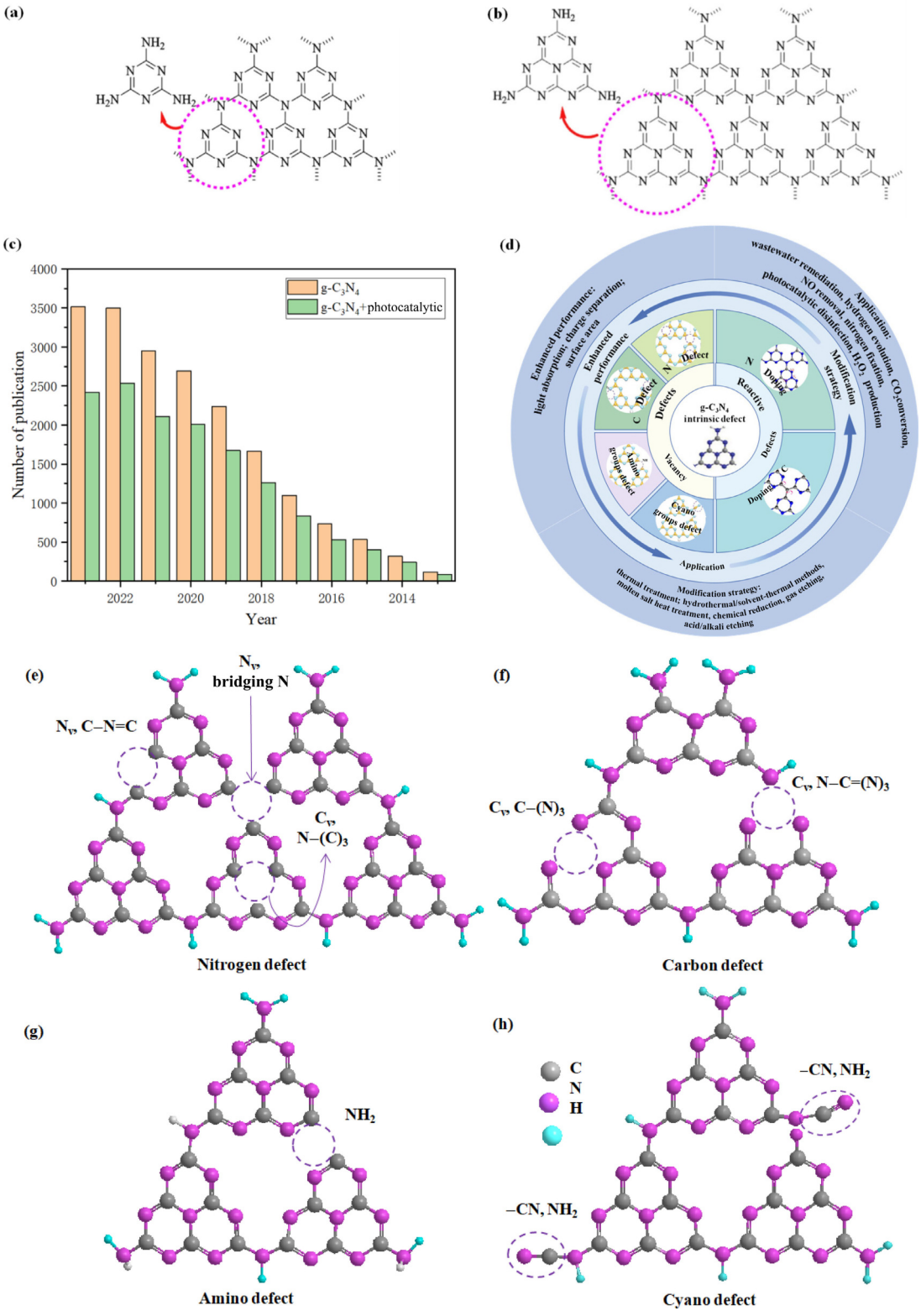

Figure 1 (a) Triazine and (b) tris-s-triazine structures of g-C_3N_4. (c) Number of articles published on topic of "g-C_3N_4" and "g-C_3N_4 + photocatalytic" from 2013 to 2023. (d) Graphical illustration demonstrates the overall aspect of this review. (e) Diagram of the typical locations of the N defect, (f) C defect, (g) amino defect, and (h) cyano defect.

chemical stability. It has been widely used in the fields of hydrogen production, CO_2 reduction, degradation of organic pollutants in water, nitrogen fixation, NO removal, and bacterial disinfection [9–12]. Given the advantages of g-C_3N_4, research interest in "graphitic carbon nitride" and "graphitic carbon nitride + photocatalytic" has shown continuingly rising trends since 2013 (Fig. 1(c)), indicating g-C_3N_4-based materials as promising metal-free photocatalysts. However, the pristine g-C_3N_4 also exhibits several disadvantages, such as limited visible light response range, less reactive sites, and high photogenerated carrier complexation rate, which need to be addressed effectively in order to meet the practical needs for environmental remediation and green new energy development [13, 14]. So far, there have been various strategies investigated, such as designing and developing heterogeneous structures, defect engineering, and morphological modulation. Among them, defect engineering has attracted much attention because it can effectively modulate the electronic band structure of photocatalytic materials, delay carrier recombination, and increase the surface reactive sites, thereby promoting the photocatalytic activity of g-C_3N_4-based materials [15–18].

In this review, the intrinsic defect types and their modification strategies are firstly discussed, and then the development and applications of intrinsic defects are reviewed in the fields of energy, environment, and health technologies (Fig. 1(d)). Additionally, the current challenges and potential solutions are outlined for intrinsic defective g-C_3N_4-based materials. It provides insights for future investigations into the design and advancement of defective g-C_3N_4-based materials.

2 Defects in g-C_3N_4

Due to the incomplete polymerization of precursors, defects are unavoidably created in the g-C_3N_4 structure [19, 20]. Previously, it was widely accepted that defects are detrimental to nanomaterials, particularly in photocatalysis, which could be detrimental to the light absorption of semiconductors and their ability to separate internal charges. However, it has recently been found that the introduction of defects is generally accompanied by a series of physical and chemical changes, such as electron localizing process, lattice distorting process and bond breaking and reformation [21], thereby altering the photocatalysts' material characteristics, energy bands and electronic structure, eventually improving the photocatalytic activity. Defective photocatalysts have shown several advantages. (1) Defects significantly affect the energy band positions. The introduction of defects generates electronic states inside the bandgap, which can reduce bandgaps or act as mid-gap states for the photoexcitation of electrons and expend the visible light absorption range [22]. (2) Defects serve as electron traps, significantly inhibiting electron-hole recombination and facilitating the migration of photogenerated charges from body to surface [23, 24]. (3) Defects are the most active activation sites of photocatalysts. The formation of defects significantly affects the electronic structure of photocatalysts, which in turn affects the activity of the reaction sites and improves the adsorption capacity and surface reaction kinetics of photocatalysts [25]. (4) Disruption of the triazine structure of g-C_3N_4, which results in the formation of voids and photocarriers [26].

According to their formation mechanisms, defects can be divided into impurity and intrinsic defects. Impurity defects refer to unintentional defects caused by the introduction of impurities (elements other than C and N) into g-C_3N_4, while intrinsic defects result from incomplete polymerization during the synthesis process. Although g-C_3N_4 with intrinsic defects maintains its original elemental composition, it exhibits internal structural deficiencies that lead to an incomplete framework [27, 28]. The intrinsic defects of g-C_3N_4 are primarily classified into two main types: vacancy defects and reactive defects. Vacancy defects contain C, N, amino and cyano functional groups, whereas reactive defects include C and N self-doping [29–31]. In general, the structure, location, and concentration of defects affect the activity of photocatalysts [20]. The defect introduction methods consist of thermal treatment, molten salt thermal treatment, hydrothermal/solvothermal method, chemical reduction, gas etching, and acid etching/alkali etching. The intrinsic defects of g-C_3N_4 are discussed below in connection with particular defects.

2.1 Defects in g-C_3N_4

2.1.1 Nitrogen defects

The nitrogen defects in N–$(C)_3$, N defects can be broadly produced by bridging N and C–N=C, which are the most common forms (Fig. 1(e)) [29, 30]. Generally, N defects can be broadly produced by chemical reduction (e.g. by H_2, $NaBH_4$, N_2H_2, and reducing solvents such as ethylene glycol and glycerol) and high temperature. Heat treatment is a special method to selectively remove specific atoms by direct calcination at high temperatures, accelerating the breaking of chemical bonds, allowing atoms to escape from the lattice and form g-C_3N_4 with a defective structure. Chemical reduction involves altering the electronic structure and properties of materials by introducing external reducing agents or solvents. This process facilitates the formation of defects on the surface or within the structure of materials, as well as the regulation of defect sites. By employing chemical reduction, researchers can achieve a more precise control over the type and distribution of defects, thereby enabling the adjustment of the material's properties. With the introduction of N defects, the visible response range can be broadened by the generation of mid-gap states. N defects can serve as electron trapping sites and active sites to improve the separation of photogenerated carriers and enhance the adsorption of g-C_3N_4 to reactants. Furthermore, the surplus electrons associated with nitrogen vacancies can interact with oxygen molecules to generate superoxide radicals. They may also associate with metallic substances to create sites for the absorption of photogenerated electrons. The synergistic effect of these above mechanisms significantly enhances the photocatalytic performance of the materials.

For example, Niu et al. [31] reduced the g-C_3N_4 layered material under an H_2 atmosphere in a temperature range of 520 to 540 °C. Without changing the basic structure of g-C_3N_4, H_2 used the interlayer channels as a diffusion pathway to produce homogeneous self-modification with N_{2c} defects. The incorporation of the N_{2c} defects narrowed the energy gap, improved the photogenerated carriers' separation efficiency, and increased the surface area of the bulk g-C_3N_4 (Fig. 2(a)). Furthermore, the g-C_3N_4 precursor was found capable of directly high temperature heating and etching with acids, bases, or gases followed by calcination to exhibit defective structure. Guo et al. [32] reported the N-defective g-C_3N_4 with porous structure in a sealed crucible using a one-step thermal polymerization method and urea precursor (Fig. 2(b)). Under the self-generating NH_3-reducing atmosphere from the urea thermal condensation process, partial N atoms were removed, resulting in N defects in g-C_3N_4. Meanwhile, the self-generating

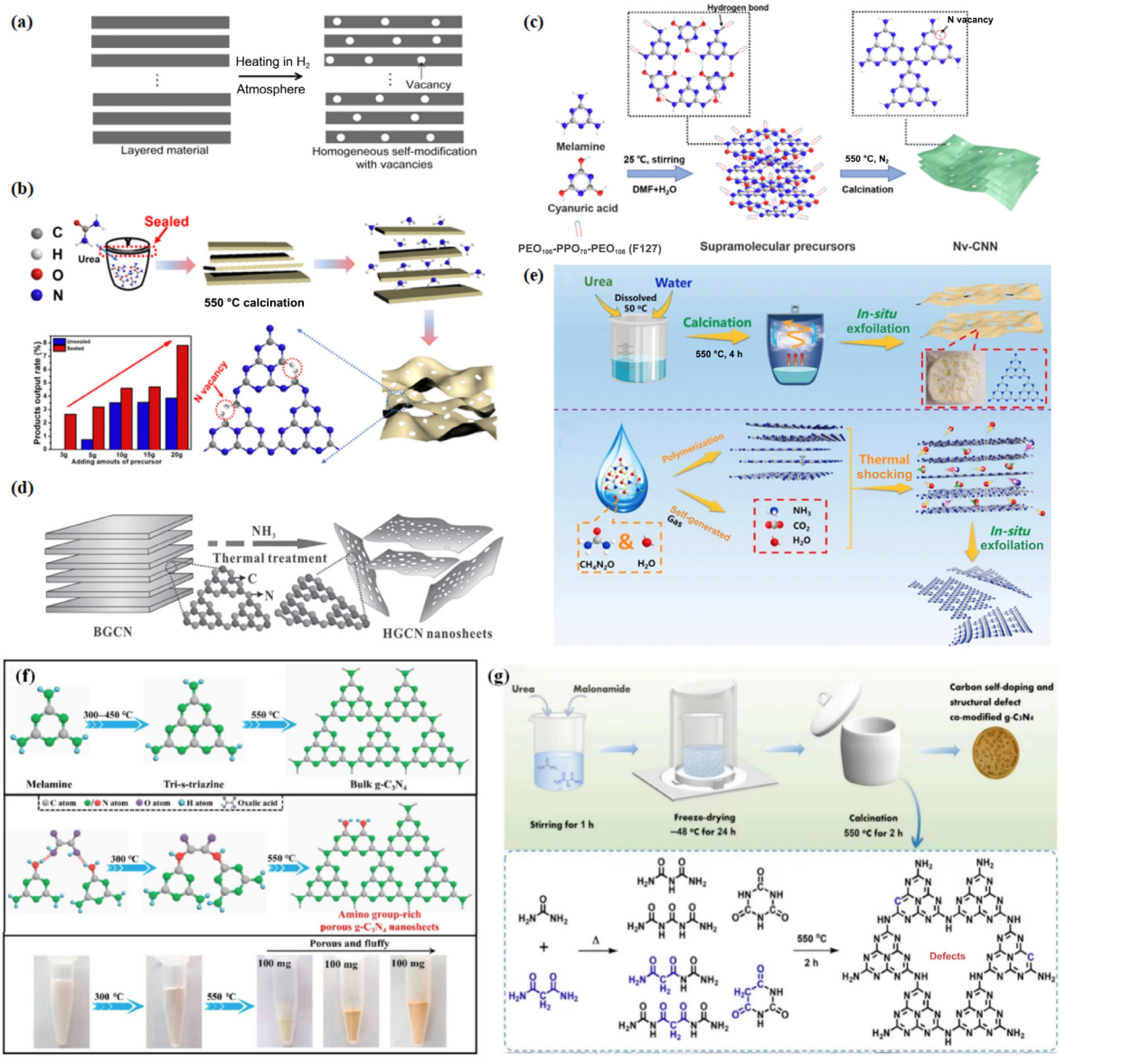

Figure 2 (a) Schematic illustration of porous N-defective g-C_3N_4. Reproduced with permission from Ref. [31], © WILEY-VCH Verlag GmbH & Co. KGaA, Weinheim 2014. (b) Schematic illustration of the preparation process of g-C_3N_4 nanosheets containing N defects. Reproduced with permission from Ref. [32], © Hydrogen Energy Publications LLC 2020. (c) Schematic of surface self-modification with defects in homogeneous self-modification with defects in a layered material after heating under H_2 atmosphere. Reproduced with permission from Ref. [33], © Elsevier Ltd. 2021. (d) Illustration of the preparation process of HGCN nanosheets. Reproduced with permission from Ref. [36], © WILEY-VCH Verlag GmbH & Co. KGaA, Weinheim 2015. (e) Schematic illustration of the synthesis of Cv-CNNs. Reproduced with permission from Ref. [37], © Elsevier B.V. 2021. (f) Graphical illustration for the synthesis of bulk g-C_3N_4 and amino group-rich porous g-C_3N_4 nanosheets (AP-CN) by direct calcination supra molecular precursor without drying. Reproduced with permission from Ref. [41], © Elsevier Ltd and Techna Group S.r.l. 2021. (g) Schematic illustration of the synthesis route and chemical structure of CDCN. Reproduced with permission from Ref. [46], © Elsevier B.V. 2023.

ammonia molecules facilitated the expansion of the aggregated g-C_3N_4 and etched the bulk g-C_3N_4 to form a porous thinner nanosheet structure, which provided more specific surface area and active site for photocatalysis. Zhao et al. [33] prepared porous g-C_3N_4 nanosheets with N_{2c} defects by high-temperature calcination using melamine and melamine acid as the raw materials. It was found that the presence of N_{2c} defects promoted the separation of electron-hole pairs and the adsorption of O_2, narrowed the energy gap, improved the separation efficiency of photogenerated carriers, and increased the surface area of bulk g-C_3N_4 (Fig. 2(c)).

2.1.2 *Carbon defects*

From a geometric perspective, carbon defects emanate from the covalent bonds breaking between carbon and nitrogen atoms with a significant number of unsaturated nitrogen atoms (Fig. 1(f)). Thus, C defects are typically situated on the C atoms that conjoin the two benzene rings or the C atoms that are close to N/NH_x. The mentioned unsaturated N atoms serve as paramagnetic centers that promote the efficient separation of electrons and holes. Moreover, the introduction of C defects can increase the valence band (VB) energy of g-C_3N_4, excite more electrons, and narrow the bandgap. Notably, C defects have the capacity to capture photogenerated electrons, thereby contributing to an enhancement in photocatalytic performance [34, 35]. The common methods for the introduction of C defects include heat treatment under different atmospheres, calcination of different precursors, hydrothermal method,

magnesium cavitation, and ultrasound-assisted thermal condensation.

Liang et al. [36] produced porous g-C_3N_4 (HGCN) nanosheets with a large number of internal pores by heat treatment of bulk g-C_3N_4 under NH_3 atmosphere. C defects were generated in the HGCN produced in this process, which gave the HGCN a broad absorption band extending into the near-infrared (NIR) region and significantly reduced the complex probability of photoexcited carriers. The Mott-Schottky plots showed that the electron donor density of HGCN was as high as 1.0%. HGCN has a high electron donor density, and the high donor density (probably caused by C defects) increases the conductivity and mobility of carriers, resulting in a photocatalytic hydrogen production rate nearly 20 times than that of bulk g-C_3N_4 (Fig. 2(d)). Gao et al. [37] developed a facile and green strategy using aqueous solution precursor for constructing surface C defects-engineered ultrathin porous g-C_3N_4 nanosheets by the direct polycondensation of urea solution under 550 °C. During the thermal polymerization process, liquid water molecules cannot only be converted into gases, but also generate more endogenous gas molecules (NH_3 and CO_2) by decomposing urea, and ultimately, under the thermally triggered gas-shock exfoliation of endogenous gases, an ultrathin g-C_3N_4 nanosheets were obtained with the four features of porous morphology, enlarged surface area (191.4 m^2/g), *in-situ* formed C defects, and edge amino groups (2 nm, about 7 g-C_3N_4 layer units). Meanwhile, the formation of C defects shifted the conduction band (CB) to a higher energy level, resulting in a stronger reduction capability (Fig. 2(e)).

The introduction of carbon vacancies in the material results in an elevation of VB, which subsequently narrows the band gap. This modification permits the excitation of electrons with reduced energy requirements. Concurrently, carbon vacancies disrupt the symmetry of the crystal structure of g-C_3N_4, leading to the formation of unsaturated nitrogen atoms within the material. These unsaturated nitrogen atoms possess unpaired electrons, enabling them to function as paramagnetic centers that can attract electrons from CB. As paramagnetic centers, the unsaturated nitrogen atoms facilitate the transfer of electrons from the conduction band to these sites, thereby enhancing the electron delocalization effect. Notably, carbon vacancies possess the capacity to capture photo-induced electrons, allowing for their mobility within the material and their participation in photocatalytic reactions.

2.1.3 *Functional groups defects*

As impacted by the incomplete condensation reaction of the N-rich precursors during the thermal polymerization, amino, cyano, and cyanamide defects are unavoidable, and these residual groups were considered as charge trap sites in the photocatalytic reaction, which adversely causes talentless charge transport and photocatalytic redox reactions affect the photocatalytic process (Figs. 1(g) and 1(h)) [38–40]. Consequently, it is imperative to enhance the photocatalytic performance of g-C_3N_4 and inhibit the recombination of photogenerated electron-hole pairs by strategically modulating the type, position, and structure of defects.

Thermal treatment is an important method for generating amino defects, which generally occur in conjunction with C defects during the thermal polymerization. Zhao et al. [41] successfully introduced amino groups into the tri-s-triazine structure units of g-C_3N_4 nanosheets via a facile oxalic acid-induced supramolecular assembly strategy. Due to the introduction of more amino groups, it can reinforce the visible-light absorption and work as the interfacial hydrogen-generation active enters to boost the photocatalytic hydrogen production (Fig. 2(f)). Clearly, cyanine groups are generally derived along with the creation of nitrogen defects, so it is also possible to introduce cyano defects into g-C_3N_4 by the thermal treatment. For example, Niu et al. [42] obtained porous g-C_3N_4 enriched with both cyano and nitrogen defects through facile 5 min thermal treatment under air, and its photocatalytic hydrogen production activity was increased by 21.5-fold compared to that of pristine g-C_3N_4. In addition, cyano defects may be incorporated into g-C_3N_4 through the pretreatment of bulk g-C_3N_4 using acids, alkalis, or salts, which is subsequently followed by a thermal treatment process. Ma et al. [43] obtained porous carbon nitride integrated with the cyano and hydroxyl functional groups through simple KCl assisted thermal treatment of urea. The density functional theory (DFT) calculation indicates that the cyano and hydroxyl groups take an important role in narrowing the bandgap, positively shifting band energy and enhancing the spatial separation of the highest occupied molecular orbital (HOMO) and lowest unoccupied molecular orbital (LUMO) states, which plausibly explains the much improved optical and electrochemical properties and the photocatalytic performance in degradation of methyl orange and NO.

2.2 Reactive site defects and their modulation strategies

Reactive site defects can arise from the exchange of lattice positions between two neighboring particles in the crystal structure. In g-C_3N_4, the primary anti-site defects are C and N self-doping. The self-doping of C and N is a self-doping modification method that can alter the intrinsic band gap structure of g-C_3N_4, leading to improve response to visible light and enhance photocatalytic activity. Moreover, the self-doping of C and N atoms can modify the electronic structure, increase conductivity, and enhance visible light absorption, thereby boosting the photo-oxidation and photo-reduction capabilities of g-C_3N_4 [44, 45].

Wang et al. [46] successfully synthesized self-doping and structural defect co-modified g-C_3N_4 (CDCN) using a thermal copolymerization method by preprocessing a mixture of urea and malonamide (Fig. 2(g)). The characterization confirmed that the absorption edges of the CDCN samples were gradually red-shifted, the band gap gradually narrowed and both CB and VB edge potentials of the CDCN shifted negatively. The above results could be attributed to the lower electronegativity C atoms that could broaden the conjugation system, narrow the bandgap, and improve the visible-light acquisition ability of CDCN. The electrochemical impedance spectroscopy (EIS) and electrostatic potential (ESP) analysis showed that the C self-doping formed an internal electric field in CDCN and accelerated the charge separation and transportation. At the same time, the simultaneous introduction of structural defects could also act as an electron-trapping center to strongly attract electrons, which effectively promoted the photocatalytic process of generation and separation of e_{CB}^- and h_{VB}^+, leading to the generation of plentiful active species.

Similarly to C doping, N doping also can improve the optical properties and photocatalytic activity of g-C_3N_4. Xing et al. [47] synthesized N-doped porous thin-walled g-C_3N_4 nanotubes (SCN) by hydrothermal and thermal polymerization methods utilizing melamine and amino urea hydrochloride as the raw materials. The experimental characterization results showed that the incorporation of nitrogen and the development of a porous structure significantly enhanced the specific surface area of the samples, and this increased

surface area facilitates the exposure of additional reaction sites, thereby promoting redox reactions and enhancing photocatalytic activity. The doping of N atoms led to the formation of midgap states and promoted the separation of charge carriers, thereby mitigating the recombination of electrons and holes. The observed downward shift of VB and upward shift of CB suggested that hydrothermal treatment and nitrogen incorporation enhanced the redox capabilities of the catalysts, facilitating photodegradation processes.

In general, the incorporation of various defect types into the g-C_3N_4 framework significantly alters its electronic structure, primarily due to modifications in the physical architecture, with the most pronounced effect being a transformation in the energy band structure. Intrinsic defects, excluding carbon-related defects, such as nitrogen and cyano defects, contribute to the narrowing of the energy bands in g-C_3N_4, thereby expanding its light absorption range and enhancing its absorption capacity. The presence of electron-rich cyano groups and nitrogen defects, which generate defect energy levels alongside carbon defects that facilitate exciton dissociation, collectively enhance carrier migration, and promote the separation of photogenerated electron-hole pairs. It is important to highlight that these defects not only modify the structure of g-C_3N_4 but also introduce coordination of unsaturated sites, which can significantly improve the adsorption and activation characteristics of g-C_3N_4, thereby facilitating photocatalytic surface reactions. However, it is crucial to recognize that the introduction of defects into g-C_3N_4 presents a dual challenge. On one hand, it enhances light absorption capability. On the other hand, it also serves as a recombination center for photogenerated carriers, leading to a reduction in their effective utilization. Furthermore, the introduction of defects may compromise the structural integrity and crystallinity of g-C_3N_4, resulting in diminished electrical conductivity and stability. Consequently, when modifying g-C_3N_4 through defect introduction, it is essential to thoroughly asses the influence of various factors, select the appropriate type of defect, and regulate the concentration accordingly.

3 Characterization of defects in g-C_3N_4-based photocatalysts

As reviewed earlier, defects provide numerous advantages for g-C_3N_4 photocatalysts, it is desirable to explain the advanced characterization technologies for defect identification to provide researchers with the knowledge they further need to explore defect materials. To date, various characterization methods have been developed to examine the defects in photocatalytic materials, but the characterization techniques for defect identification still present great challenges.

We summarize the characterization techniques for defective g-C_3N_4 (Table 1), and classified the existing techniques into microscopic characterization and spectroscopic characterization. The characterization methods for defects in photocatalytic materials are dependent on the types of defects. Generally, microscopic techniques can observe the defects that cannot be seen with the naked eyes, which represent the most direct and widespread way to have insights into defects [48–50]. There are many kinds of microscopes suitable for the observation of various defects, such as scanning electron microscopy (SEM), transmission electron microscopy (TEM), as well as atomic force microscopy (AFM). Although microscopic techniques can identify the defects according to lattice irregularity or impurity composition, spectroscopic techniques are indispensable to resolve the detailed atomic structures of defects in photocatalytic materials. For effectual inspection of chemical changes produced in g-C_3N_4 due to defect engineering, X-ray photoelectron spectroscopy (XPS) and Fourier transformation infrared (FTIR) spectroscopic analysis are very advantageous. Besides, other analysis techniques used to investigate the chemical composition of a sample, involving X-ray absorption fine structure (XAFS), electron spin resonance (ESR) and positron annihilation spectroscopy (PAS) played a significant role in the characterisation of defect rich photocatalysts. XAFS spectroscopy is particularly suitable to study the atomic coordination number, structural disorder and other structural information in the defective

Table 1 Summary of various characterisation techniques with their advantages and disadvantages used to identify defects in g-C_3N_4

Characterisation technique	Advantage	Disadvantage
STEM/HRTEM	Provides intuitive visualization of surface reorganization by defect generation.	The amount and exact position of vacancy defects cannot be measured.
Scanning tunneling microscopy (STM)	Identify the surface structure and composition of defects; reveal the surface morphology.	Low sensitivity; lacking detailed structural change.
XRD	Detecting the crystalline shape of a material.	Low sensitivity, needs more coupled methods.
FTIR	Present the changes in chemical bonding of chemical compositions due to the formation of defects.	Low sensitivity, needs more coupled methods.
X-ray photoelectron spectroscopy (XPS)	Reveal changes in chemical state by the formation of defects; provides information on the defect type, chemical state, composition, defect concentration and band structure.	Only reflect semi-quantified information of surface defects. Inaccurate surface analyses.
Raman spectrometry	Directly reflect defects by the various group configurations and chemical bonds.	Needs more coupled methods.
EPR	Qualitative and quantitative analysis of defect types and concentrations.	Inability to present information on structural changes after the formation of defects.
PAS	High sensitivity; provide the defect structures at the atomic level of materials, such as number, size, concentration (down to ppm levels) and changes of the defect.	For certain types of defects, the sensitivity may not be high enough to accurately detect the relevant information.

2D materials, so as help to probe the atomic defects, which is one of the most important methods for examining the local atomic arrangements of defects in photocatalytic materials [51]. PAS is another powerful technique for investigating defects in photocatalytic materials, which has been demonstrated to be useful to distinguish the intrinsic defects in semiconductors [52, 53]. Therefore, the defects types and relative concentration can be distinguished by measuring the different positron lifetimes. For instance, Guo et al. [54] synthesized N defects g-C_3N_4 by calcining $NaBH_4$ (sodium borohydride) and precursor of g-C_3N_4. The X-ray diffraction (XRD) shows that the introduction of N defects has no effect on the crystal structure of g-C_3N_4, and the peak of interlayer stacking of the C–N conjugated aromatic units is decreased obviously, which is due to the introduction of N defects. The FTIR spectroscopy revealed more about the molecular frameworks of the defective porous g-C_3N_4 nanotube (DTCN) and the initial g-C_3N_4 nanotube (TCN). The peaks were detected at 2170 cm^{-1}, which corresponds to the asymmetric stretching vibration of the cyano group (C≡N). This result indicates that the N–H groups on the surface may be replaced by C≡N groups during the pyrolysis process, suggesting the presence of defects. Moreover, SEM and TEM micrographs were used to recognize defects in g-C_3N_4 nanospheres, it shows that both DTCN and TCN have a uniformly distributed porous hollow tubular structure and the morphology of nanotubes can still be maintained, which proves that the nanotubes are successfully obtained. The TEM images shows that DTCN exhibits more porosity. Reasonably, the porous hollow structure offers abundant surface active sites, which is conducive to improving the photocatalytic performance.

4 Applications of intrinsically defective g-C_3N_4-based photocatalysts

The modification strategy applied to defective g-C_3N_4 has significantly advanced the performance of g-C_3N_4-based materials in terms of light absorption, charge transfer efficiency, and surface reaction kinetics. This progress has heightened interest in their applications for photocatalytic hydrogen production, organic degradation, photocatalytic denitrification, and bacterial disinfection. It is important to highlight that g-C_3N_4 with various types of defects exhibits distinct effects on photocatalytic performance. Here, some representative examples are presented and discussed to elucidate the specific mechanisms by which the introduction of different defects enhances photocatalytic activity across various applications. This analysis aims to inspire further exploration of defect-modified g-C_3N_4 and deepen our understanding of the photocatalytic mechanisms associated with intrinsic defect types.

4.1 Wastewater remediation

Long-term presence of organic pollutants such as pesticides, antibiotics and organic dyes in water bodies, which have caused great harm to human beings and the environment. While the photocatalytic degradation of these pollutants utilizing g-C_3N_4 has achieved some remarkable results in wastewater treatment, several limitations, and challenges persist. Abundant studies have indicated that intrinsic defects within the material can serve as active sites for photocatalytic water oxidation reactions, thereby enhancing the degradation of pollutants and demonstrating superior efficacy in the photocatalytic degradation of organic pollutants compared to pristine g-C_3N_4 [55–58].

The introduction of C defects into g-C_3N_4 could greatly improve its photocatalytic efficiency by providing a distinctive site for trapping photo-induced electrons, thereby facilitating the effective separation of electron-hole pairs. Liang et al. [59] successfully synthesized C defects-modified g-C_3N_4 (V_C-C_3N_4) via a handy two-step calcination method and firstly applied in the photocatalytic removal of bisphenol A (BPA). Compared to pristine g-C_3N_4, the photocatalytic removal of BPA over V_C-C_3N_4 reached 90.0% in 420 min illumination, and the kinetic constant k of BPA degradation was 1.65 times higher than that of the pristine g-C_3N_4. The enhanced photocatalytic performance of V_C-C_3N_4 was primarily attributed to the critical role of C defects. These defects enhance electrophilicity, allowing for the rapid capture of photogenerated electrons, which inhibits the recombination of photogenerated holes and electrons. This process facilitates the migration of electrons to the surface of V_C-C_3N_4, where they can participate in the photocatalytic reaction. Additionally, the C defects serve as conversion centers, transferring the captured electrons to adsorbed O_2, thereby generating a substantial amount of superoxide radicals ($-O_2^-$), which play a crucial role in the photocatalytic degradation mechanism (Figs. 3(a)–3(c)).

The introduction of N defects can accelerate the separation of photogenerated electron-hole pairs, resulting in electron-deficient effects. This enhancement has subsequently increased the hydrophilicity of g-C_3N_4. The augmented hydrophilicity is expected to lower the activation energy associated with water diffusion and dissociation, thereby promoting water adsorption and the subsequent of water oxidation process. Li et al. [60] successfully synthesized N defects engineered reticulate g-C_3N_4 (Nv-RCN) for the photodegradation of propyl hydroxybenzoate (PrP). Compared with bulk g-C_3N_4, Nv-RCN exhibited larger specific surface area, stronger light absorption, higher carrier transfer and separation efficiency. The removal of PrP by Nv-RCN was 94.3%, and the corresponding apparent rate constant of Nv-RCN was 3.37 times higher than that of bulk g-C_3N_4. The possible reaction mechanism is as follows. The reticular nanostructure significantly enhances the specific surface area and the absorption range of visible light, which could increase the availability of active reaction sites and facilitate the generation of more electron-hole pairs. Furthermore, N defects served as electron trapping sites to promote the O_2 adsorption and accelerate the separation of photogenerated charge carriers, leading to the production of more reactive oxygen species. Electrons on shallow trapping sites could react with the adsorbed O_2 on the surface of Nv-RCN to produce a substantial quantity of superoxide radicals ($-O^{2-}$). Simultaneously, the holes could oxidize partial $\cdot O^{2-}$ to generate $^1O_2$ and a small amount of ·OH. As a result, PrP molecules are activated by these reactive species under solar irradiation through various processes, including decarboxylation, decarbonylation, dealkylation, and ring-opening, which caused the rapid degradation within a short time (Figs. 3(d)–3(f)). Additionally, the co-modification of g-C_3N_4 with N and C defects can induce a synergistic effect that optimizes the energy bands and electronic structure of g-C_3N_4, significantly enhancing its photocatalytic oxygen production activity.

Zhang et al. [61] introduced both C and N defects into g-C_3N_4 microrods by facial thermal polymerization of melamine-cyanuric acid supramolecular (MCS) precursors under H_2 atmosphere (H-CN). Concurrently, they synthesized argon-derived carbon nitride (Ar-CN) with N defects and microwave-prepared carbon nitride (M-CN) with C defects using analogous methodologies under argon and microwave conditions, respectively. With the combined

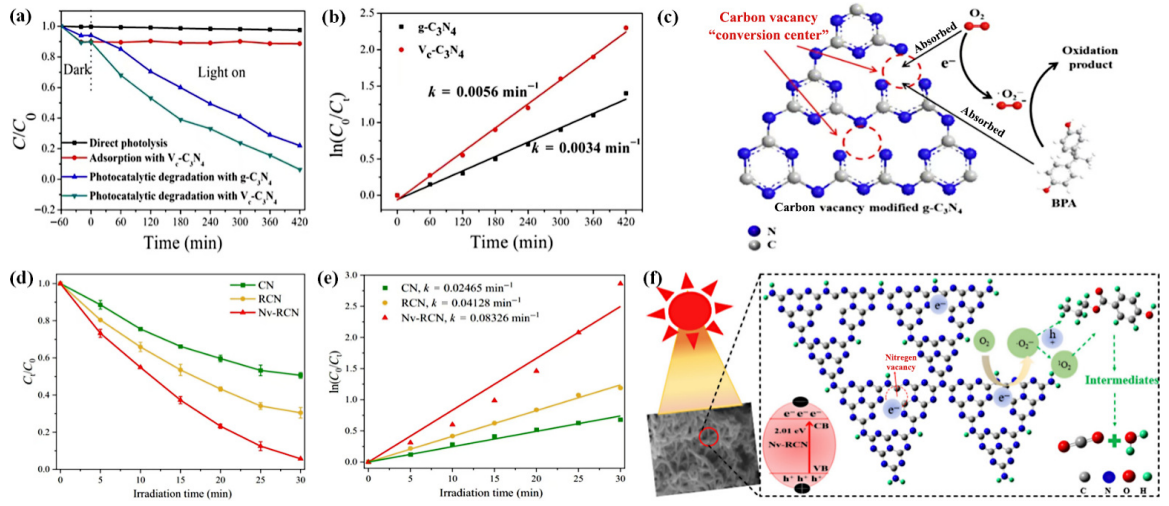

Figure 3 (a) The degradation of BPA and (b) kinetic constants with g-C_3N_4 and V_C-C_3N_4 under visible light; (c) the action mechanism of V_C-C_3N_4 under visible light irradiation. Reproduced with permission from Ref. [59], © American Chemical Society 2018. (d) Removal efficiency, and (e) corresponding kinetic curves of PrP on CN, RCN, and Nv-RCN; (f) schematic illustration of the enhanced photodegradation mechanism of PrP on Nv-RCN. Reproduced with permission from Ref. [60], © Elsevier B.V. 2022.

characteristics, the photocatalytic performance of HCN, Ar-CN, and M-CN was significantly improved, and the degradation kinetic constants (k) of RhB for 15, 50, and 60 min were 0.19363, 0.05674, and 0.0429 min^{-1}, respectively, which were 16.52, 4.84, and 3.66 times higher than those of pristine g-C_3N_4. SEM and TEM analysis showed that H-CN has a larger specific surface area (31.384 m^2/g, which is 7.2 times greater than that of the pristine g-C_3N_4) and porous structure, which could provide more reactive sites for photocatalytic reactions and more channels for carrier migration and substance transport. Furthermore, photoelectric property assessments demonstrated that the introduction of C and N defects effectively reduced the bandgap of H-CN to 2.43 eV, which effectively enhanced the absorption of visible light. Additionally, both C and N defects served as electron traps, which increased the electron density and inhibited the recombination of photogenerated electrons and holes. Moreover, both C and N defects can be used as oxygen adsorption sites, which promotes the transfer of photogenerated electrons to the oxygen reduction sites and facilitates the generation of the key active substance ($\cdot O_2^-$), thereby improving the photocatalytic activity.

Currently, the research direction is focused on identifying more efficient alternative materials or enhancing the performance of existing materials to further improve the pollutant removal efficiency, satisfy industrial requirements, and mitigate their potential environmental impact.

4.2 Hydrogen evolution

In recent years, g-C_3N_4 has attracted much attention in photocatalytic hydrolysis for hydrogen production. Although the pristine g-C_3N_4 can catalyze water reduction for hydrogen production under visible light irradiation, production rates are low and unsatisfactory for industrial production. This is mainly due to the limited visible light absorption range, low photogenerated electron separation rate, and small specific surface area of g-C_3N_4, which result in its insufficient photocatalytic hydrogen precipitation activity. Research has demonstrated that the introduction of defects can alter the position of VB in g-C_3N_4 and reduce its intrinsic band gap during the photocatalytic hydrogen production process [62–67].

Notably, the incorporation of N defects can create mid-gap states at the edge of the conduction band, which facilitates carrier migration, significantly reduces the recombination of electron-hole pairs, and broadens the photoresponsive range of g-C_3N_4. As a result, these alterations enhance the photocatalytic performance of the material. Qin et al. [68] integrated N defects and π-conjugated structure into g-C_3N_4 (DCN350) by low-temperature calcination of g-C_3N_4 and $NaBH_4$ for application in hydrogen evolution. The photocatalytic hydrogen evolution rate of DCN350 was 1541.6 μmol/(g·h), which was 7.5 times higher than that of pristine g-C_3N_4 (205.9 μmol/(g·h)) (Figs. 4(a) and 4(b)). Compared with pristine g-C_3N_4, N defects can evidently narrow the band gap of g-C_3N_4 (1.69 to 0.99 eV) for expanding the visible light absorption due to the formation of mid-gap state, and also act as active sites for promoting hydrogen evolution reactions. In addition, the formation of cyanine (–C≡N) can act as a strong electron-withdrawing functional group, which promotes the departure of isolated valence electrons from the domains and accelerates the charge-separation transfer. Finally, the H_2O adsorbed on the surface of g-C_3N_4 reacts with electrons to form H_2 and OH^-, while H_2 is desorbed from the active sites and diffuses through the porous structure.

N defects, cyano and porous structures of the DCN350 photocatalyst synergistically promote efficient H_2 reaction (Fig. 4(c)). Shan et al. [69] successfully synthesized a tubular g-C_3N_4 photocatalysts containing N defects and cyano π-conjugated structure through thermal polymerization (AIL-2.0-CN). The photocatalytic hydrogen evolution rate of AIL-2.0-CN was 1284 μmol/(g·h) with an apparent quantum efficiency of 4.2%, which was 13.6 times higher than that of pristine g-C_3N_4. The combination of N defects and heteroatom-doping modified g-C_3N_4 was also profiled to be an auspicious way to improve its photocatalytic ability effectively. Wang et al. [70] designed a novel N-deficient and S-doped g-C_3N_4 material (S-g-C_3N_4-D). The physical and chemical characterization showed that S-g-C_3N_4-D not only had a 2D lamellar appearance with large porosity and a high specific surface area but also had efficient light-utilization and carrier separation and transfer capabilities. S-g-C_3N_4-D showed a high hydrogen evolution rate (5651.5 μmol/(g·h)) (Figs. 4(d) and 4(e)), which can be attributed to its elevated specific surface area

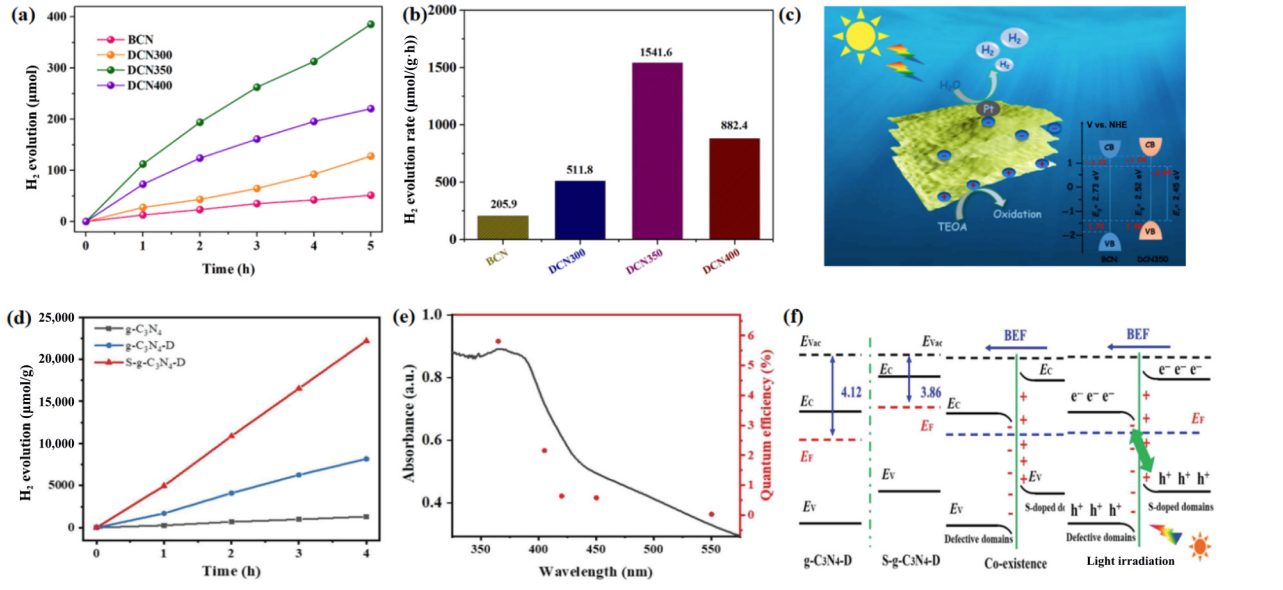

Figure 4 Time courses of photocatalytic H_2 evolution of the as-prepared samples (a) and photocatalytic H_2 evolution rate of BCN and DCN nanosheets under visible light irradiation (b); (c) proposed mechanism of H_2 evolution by the DCN350 under visible light. Reproduced with permission from Ref. [68], © Elsevier B.V. 2021. (d) Dates of photocatalytic H_2 evolution of g-C_3N_4, g-C_3N_4-D, and S-g-C_3N_4-D; (e) AQE of S-g-C_3N_4-D; (f) formation process of build-in electric field (BEF) and charge transfer mechanism of defective g-C_3N_4/S-doped g-C_3N_4 step-scheme heterojunction. Reproduced with permission from Ref. [70], © Wiley-VCH GmbH 2023.

and considerable total pore volume, providing numerous active sites for the reaction and enhancing the transfer efficiency of photogenerated carriers. This, in turn, augmented the photocatalytic activity for hydrogen production via water electrolysis. Additionally, the incorporation of N defects and S atoms can narrow the band gap (2.68 eV) to significantly enhance the visible light absorption and response-ability, and the two acted as electron trapping traps, which can effectively inhibit the compounding of photogenerated electron-hole pairs, and the separation, transfer and recombination ability of photogenerated carriers (Fig. 4(f)). Finally, a step-scheme heterojunction was established between the N defects and S atomic domains within g-C_3N_4, which significantly enhanced the photocatalytic hydrogen evolution rate.

The introduction of C defects can also improve the photocatalytic performance of g-C_3N_4. Gao et al. [37] prepared ultrathin g-C_3N_4 photocatalysts (U1W1-CNS) by a thermally triggered *in-situ* gas-shock method utilizing endogenous gases (CO_2, H_2O, and NH_3) from urea solution. The optimal photocatalyst, U1W1-CNS, was an ultrathin structure (2 nm thickness) with abundant C defects in the porous state, thereby endowed with excellent structural properties (191.4 m^2/g, 0.61 cm^3/g), which not only enlarged its special surface area to accommodate more reaction sites but also shortened the carrier migration distance. At the same time, the presence of C defects served to inhibit the recombination of photogenerated carriers, while simultaneously elevated the conduction band of U1W1-CNS to a higher energy level. This shift facilitated more vigorous redox reactions, thereby enhancing catalytic activity. Additionally, the hydrophilicity of U1W1-CNS was significantly improved due to the increased presence of amine functional groups at the edges of the structure, which enhanced its dispersibility in aqueous environments and substantially improved visible light absorption. Consequently, the synergistic interplay between C defects and the ultrathin nanoporous architecture culminated in the exceptional photocatalytic performance of U1W1-CNS, achieving a hydrogen production efficiency of 10.14 mmol/(g·h), which was 57 times higher than that of the unmodified g-C_3N_4. Moreover, the incorporation of C defects and S-atom doping in the modified g-C_3N_4 material can further augment its photocatalytic efficacy. S-doped and C-defective honeycomb g-C_3N_4 nanosheets(S-PDCN) were synthesized by Tian et al. [71]. The doping of S atoms not only significantly enhanced the specific surface area of g-C_3N_4 but also modified the bandgap structure. Furthermore, the introduction of C defects increased the number of reactive sites, broadened the range of visible-light responsiveness, and facilitated photogenerated the separation and transfer carriers. The experimental results indicated that S-PDCN-3 exhibited the highest hydrogen production efficiency at 23.78 mmol/(g·h), which was 21.8 times greater than that of pure g-C_3N_4, which had an efficiency of 1.1 mmol/(g·h).

4.3 CO_2 conversion

Achieving carbon neutrality is an urgent global challenge to address the energy and environmental issues for sustainable development. Photocatalytic CO_2 conversion can convert CO_2 into high-value-added chemical raw materials and fuels by utilizing solar energy, and is considered to be one of the most feasible technologies to solve the energy crisis and environmental problems. g-C_3N_4, a typical conjugated polymer, is one of the most attractive and promising photocatalysts due to its unique conjugated structure, low cost, simple preparation, and visible light response. However, the serious exciton effect, the difficulty in separating electron-hole pairs, and poor CO_2 adsorption capacity greatly limit the photocatalytic activity of g-C_3N_4 [72–74]. A potential solution to these issues may involve optimizing the surface properties and energy band structure of g-C_3N_4 through intrinsic defect engineering.

The CO_2 adsorption capacity of a photocatalyst plays a prevailing role in catalyzing CO_2 reduction. Resent work in this area proved that intrinsic defect engineering can significantly increase the adsorption and conversion of CO_2 by g-C_3N_4 [75–80]. The

presence of N defects can significantly enhance the electrondensity of nearby atoms, which can significantly enhance the adsorption of CO_2 by g-C_3N_4. For instance, Liu et al. [81] employed the N defect hollow microtubule-structured g-C_3N_4 (TCN) by hydrothermal self-assembly followed by H_2 heat treatment. TCN exhibited excellent activity for photocatalytic CO_2 reduction, giving the CO generation rate of 7.06 mmol/(g·h) without any co-catalyst or sacrificial agent, which was 8.8 times higher than that of pristine g-C_3N_4 (0.75 mmol/(g·h)) (Figs. 5(a)–5(c)). DFT calculations showed that the N defects promote CO_2 adsorption and activation. The excellent photocatalytic CO_2 reduction performance can be attributed to multiple factors. (1) The porous one-dimensional hollow tubular structure improves the efficiency charge separation and provides abundant active centers for the surface reaction. (2) The introduction of N defects not only generates a localized disordered structure but also acts as an electron trap to promote exciton dissociation into free charge, and generates a strong Lewis alkalinity, which is beneficial to the activation of CO_2 adsorption, thereby promoting the CO_2 photocatalytic reduction (Fig. 5(d)). g-C_3N_4 photocatalysts with N defect porous structure were prepared by Ma et al. [82] using *in-situ* doping and freeze-drying. It enhanced photo-reduction CO_2 performance with CO and CH_4 productivity about 19.7 and 37.1 μmol/g, respectively, which were 4.8 and 3.8 times higher than those of bulk g-C_3N_4. The experimental and DFT theoretical calculation results indicated that the synergistic effect of unique porous and the N-defect structure significantly can facilitate the photoreductive CO_2 performance and affect the CO and CH_4 conversion rates.

The surface groups formed by C defects can adsorb CO_2 more easily than N defects, and the defects can promote the separation of electron-hole pairs, providing more adsorption and activation sites for the reactant molecules, thereby promoting the effective reduction of CO_2. Nor et al. [83] used glucose as a carbon source and urea as a precursor to thermally polymerize g-C_3N_4 (C/g-C_3N_4) catalysts with C self-doped layered porous structure in photocatalytic reduction of CO_2 to CH_3OH under ultraviolet–visible (UV–Vis) light irradiation. During the photocatalytic performance test, the highest methanol yield of C/g-C_3N_4 was up to 651.7 μmol/(g_{cat}·h) with apparent quantum yield (AQY) = 0.019, representing an approximate 40% enhancement relative to the pristine g-C_3N_4. This improvement was attributed to the nanorod structure of C/g-C_3N_4, which provided higher surface area and more active sites, thereby enhancing the adsorption between CO_2 and the photocatalyst (Fig. 5(e)). Moreover, the substitution of N sites with C atoms at a defect concentration of 12.7% can effectively improve the electron-hole pair separation

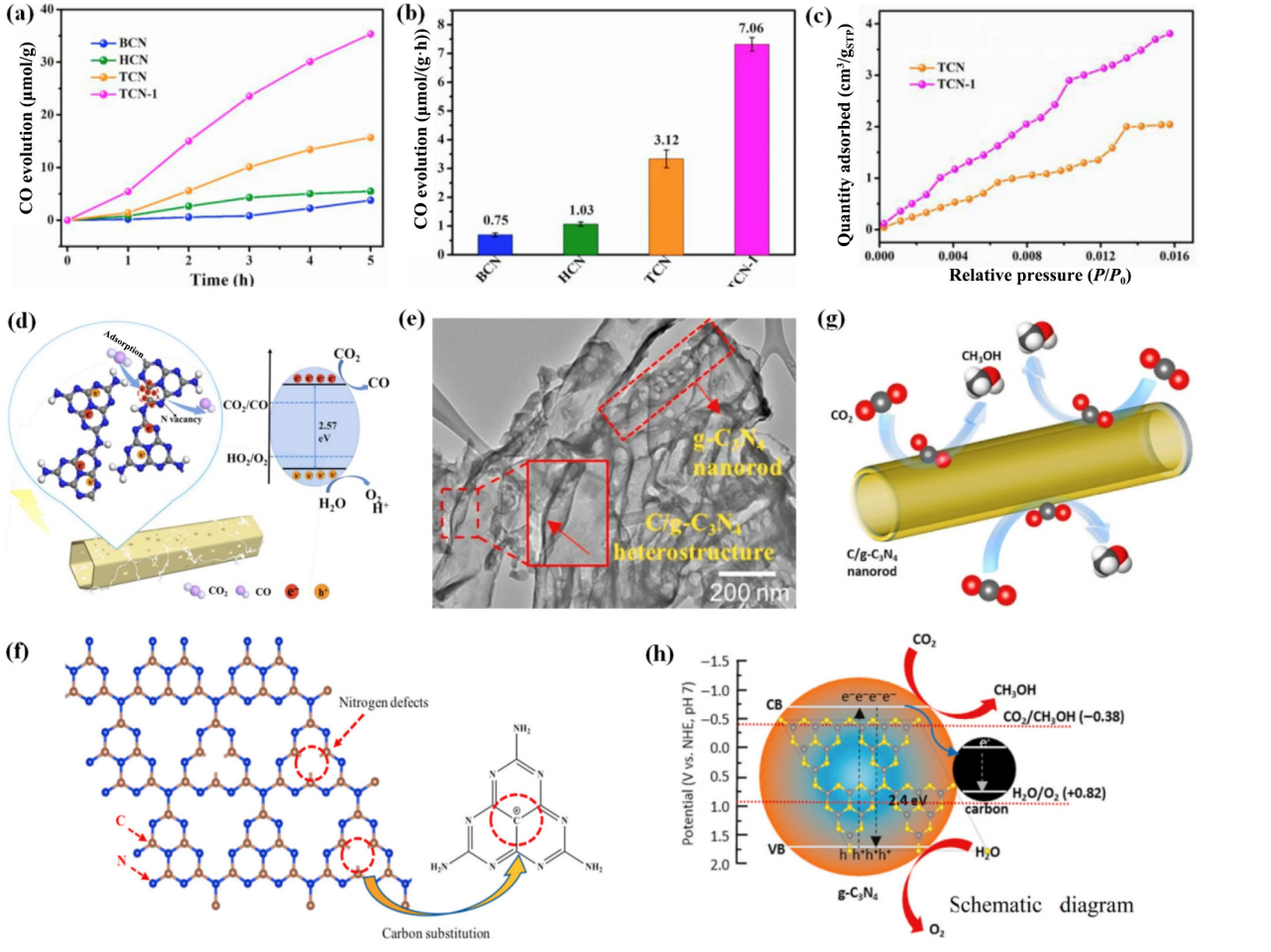

Figure 5 (a) Time-dependent photocatalytic CO evolution curves; and (b) average CO evolution rate of BCN, HCN, TCN, and TCN-1 under 350–780 nm light irradiation; (c) CO_2 adsorption curves of TCN and TCN-1; (d) mechanism of photocatalytic reduction of CO_2 by TCN-1. Reproduced with permission from Ref. [81], © Elsevier Ltd. 2022. (e) SEM image of 0.2C/g-C_3N_4; (f) schematic illustration of C atom replacing N atom in 0.2C/g-C_3N_4; schematic diagram of (g) the interaction between CO_2 molecule and surface area of C/g-C_3N_4 nanorods, and (h) mechanism of photo-generated charge carrier separation in C/g-C_3N_4. Reproduced with permission from Ref. [83], © Elsevier B.V. 2021.

efficiency and photocatalytic activity. Furthermore, the formation of C defects at the CN1 sites also contributed to extending the light absorption and reducing the band gap of the photocatalyst, which effectively reduced the recombination rate of the photogenerated carriers while maintaining a substitution (Figs. 5(f)–5(h)).

4.4 NO removal

NO absorbed on the surface of the photocatalyst is oxidized by $\cdot O_2^-$, ·OH, and positive holes (h^+), ultimately resulting in the formation of NO_3^- via intermediates such as NO_2 and HNO_2 (Eqs. (1)–(7)). Although g-C_3N_4 exhibits superior photocatalytic properties and pristine g-C_3N_4 demonstrates moderate efficacy in removing nitric oxide from the atmosphere (with a removal rate of only 21.2% for bulk carbon nitride), its effectiveness is hindered by several factors. These include its limited capacity for the adsorption and activation of both O_2 and NO, low absorption of visible light, and a high rate of electron-hole recombination. Consequently, g-C_3N_4 is not proficient in removing nitrogen oxides [84–86]. The incorporation of defective structures has the potential to address these limitations, facilitating the complete oxidation of NO to HNO_3 and thereby enhancing the removal efficiency of nitrogen oxides [87–91].

$$\text{Photocatalyst} + h\nu \rightarrow e^- + h^+ \quad (1)$$

$$O_2 + e^- \rightarrow \cdot O_2^- \quad (2)$$

$$h^+ + OH^- \rightarrow \cdot OH \quad (3)$$

$$NO_x + \cdot O_2^- \rightarrow NO_3^- \quad (4)$$

$$NO + \cdot OH \rightarrow HNO_2 \quad (5)$$

$$HNO_2 + \cdot OH \rightarrow NO_2 + H_2O \quad (6)$$

$$NO_2 + \cdot OH \rightarrow NO_3^- \quad (7)$$

The design of C defects in g-C_3N_4 is important. Dong et al. [92] synthesized ultrathin g-C_3N_4 nanosheets with C defects (Ns-g-C_3N_4) through the calcination of melamine and cyanuric acid in a sealed crucible at 550 °C. They subsequently evaluated the photocatalytic efficacy of these nanosheets for the reduction of NO.

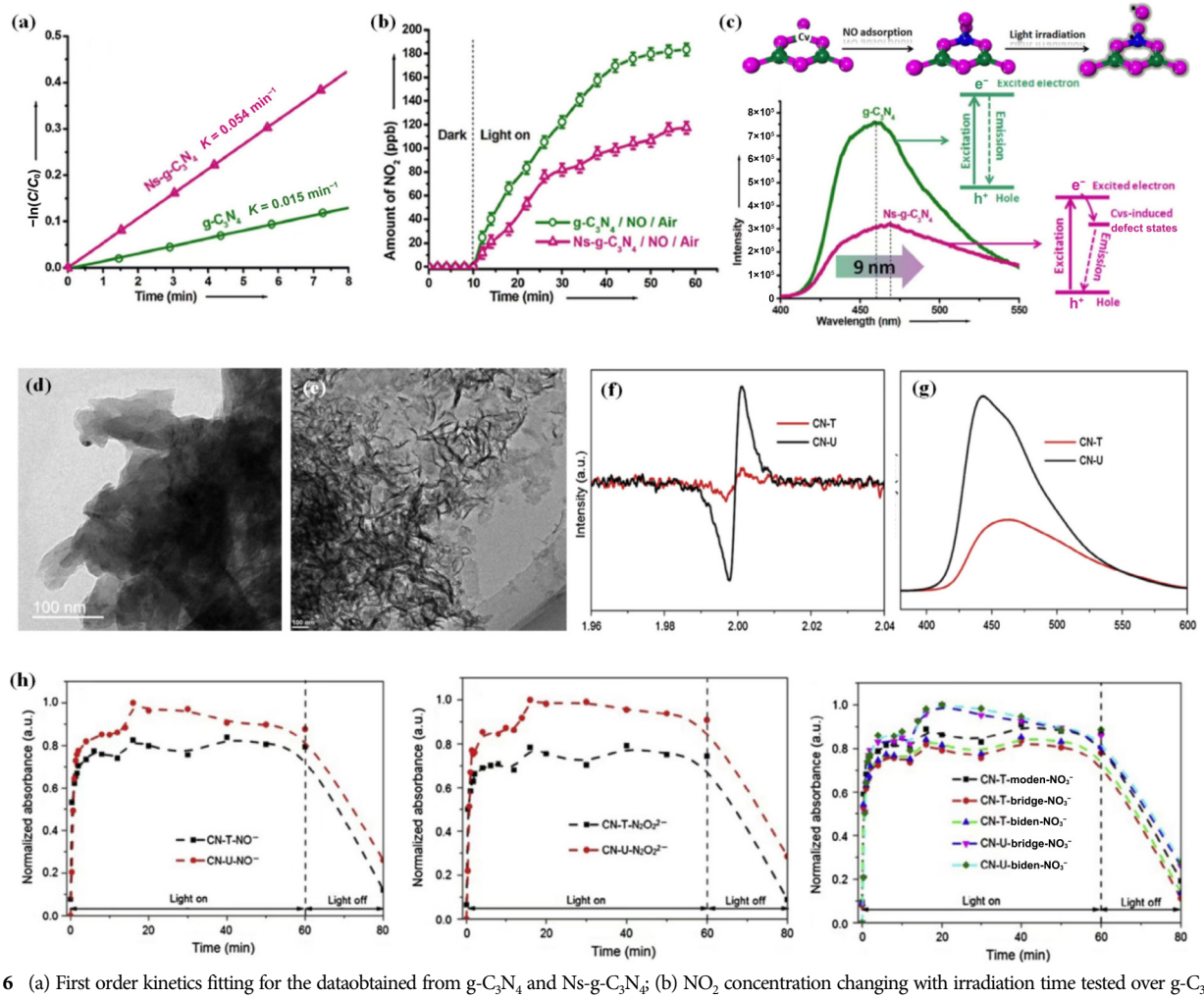

Figure 6 (a) First order kinetics fitting for the dataobtained from g-C_3N_4 and Ns-g-C_3N_4; (b) NO_2 concentration changing with irradiation time tested over g-C_3N_4 and Ns-g-C_3N_4; (c) photoluminescence spectrum of the g-C_3N_4 and Ns- g-C_3N_4 and the decomposition process of NO on the surface of Ns- g-C_3N_4. Reproduced with permission from Ref. [92], © Elsevier B.V. 2017. (d) and (e) TEM images of CN-T and CN-U; (f) N_2 adsorption–desorption isotherms and (g) pore size distribution curves of CN-T and CN-U; (h) normalized absorbance of adsorbed NO^- on CN-T and CN-U, $N_2O_2^{2-}$ on CN-T and CN-U and NO_3^- on CN-T and CN-U as a function of time during photocatalytic NO. Reproduced with permission from Ref. [93], © Science China Press 2017.

While g-C_3N_4 was capable of photo-oxidizing NO to NO_2, Ns-g-C_3N_4 demonstrated the ability to photoreduce NO to environmentally benign N_2 with a conversion efficiency of 66% (Figs. 6(a) and 6(b)), marking the highest reported conversion rate of NO to N_2 under visible light irradiation to date. The study identified two critical structural characteristics of Ns-g-C_3N_4, including its ultrathin nanostructure and the presence of numerous surface defect sites, which were advantageous for enhancing visible light absorption, facilitating the separation and transfer of photogenerated charge carriers, and promoting the strong chemisorption of NO, all of which contributed to its elevated photoreactivity. Furthermore, the C defects present on the surface of Ns-g-C_3N_4 served as electron traps for capturing photogenerated electrons while simultaneously providing preferential adsorption sites for NO. This spatial proximity of photogenerated electrons and NO molecules enabled direct electron transfer from the defect sites to NO, ultimately resulting in the reduction of NO to N_2 and O_2 (Fig. 6(c)).

It was also demonstrated that introducing N defects optimized the energy band structure and increased the light absorption capability of g-C_3N_4, which resulted in stronger adsorption of NO by N defects and provided a specific location for the reactant molecules. Furthermore, these defects can function as electron trapping centers, thereby diminishing the electron-hole recombination rate. Consequently, the photocatalytic oxidation activity of NO in g-C_3N_4 can be markedly enhanced through the introduction of N defects. Wang et al. [93] prepared g-C_3N_4 with different structures by heat treatment under the same conditions using urea (CN-U) and thiourea (CN-T) as the precursors. The microstructures and optical properties were characterized. The results showed that compared with CN-T, the porous and high specific surface area of CN-U favored the adsorption of pollutants on the photocatalyst surface (Figs. 6(d) and 6(e)), the wide bandgap facilitated the redox capacity, and the N defects facilitated the effective separation of photogenerated charges (Figs. 6(f) and 6(g)). Meanwhile, the adsorption and reaction process of visible light-catalyzed oxidation of NO on g-C_3N_4 were monitored by the *in-situ* FT-IR technique. The main intermediates produced during the reaction were NO^- and $N_2O_2^{2-}$, and the final product was NO_3^-. Figure 6(h) exhibits a dynamic equilibrium for the relative contents of CN-T and CN-U final products, which further indicates that CN-U has a stronger NO oxidizing ability. The main reasons likely include: (1) The presence of defective sites that facilitates the adsorption of gas molecules while being electronic compensated leading to promoting the formation of final products; (2) the high separation efficiency of photogenerated electron-hole pairs that promotes the generation of free radicals during the photocatalytic reaction; and (3) the ·OH that are not selective for pollutant decomposition, which can directly oxidize NO and negatively charged intermediates to generate more stable NO_3^-. The synergistic effect of N deficiency and other modifications could just as well improve the removal of NO by g-C_3N_4 photocatalysis.

Overall, the modified g-C_3N_4 materials have showed significant enhancement in photocatalytic activity by introducing defects and modulating the morphology, especially for NO conversion reactions. These studies also provide a feasible strategy for further improving the design of photocatalytic materials.

4.5 Nitrogen fixation

The production of ammonia holds considerable significance for both industrial advancement and agricultural fertilization. Currently, the conventional Haber–Bosch process remains predominant for artificial nitrogen fixation. This process is conducted in a high-pressure reactor, operating at elevated temperatures ranging from 400 to 450 °C and pressures between 150 and 200 atmospheres. However, it is noteworthy that this method requires substantial energy input and contributes significantly to greenhouse gas emissions [94]. Therefore, there is an urgent need to find an environmentally friendly way to synthesize ammonia artificially. Photocatalytic nitrogen fixation is a promising clean technology that utilizes semiconductor materials to absorb solar energy and generate electrons and holes. The photogenerated electrons can reduce inert nitrogen molecules to ammonia under mild conditions [95]. Nonetheless, the high reduction potential required for converting nitrogen to ammonia limits the availability of suitable catalysts. Additionally, the sluggish reaction kinetics of inert N_2 molecules on the catalyst surface results in low N_2 fixation efficiency. The g-C_3N_4 as a novel metal-free photocatalyst, possesses a conduction band potential that exceeds the reduction potential of N_2/NH_3, thereby enabling the reduction of N_2 to NH_3 under visible light irradiation [96–99]. However, the photocatalytic activity of g-C_3N_4 is hindered by its limited specific surface area, a high recombination rate of photogenerated electron-hole pairs, and weak chemisorption of N_2. Recent literature has reported various strategies for designing g-C_3N_4-based photocatalysts for nitrogen fixation, which can regulate the adsorption/desorption of the reactants/products, lower the reaction energy barrier, and inhibit the competing reactions, which is favorable for the uptake of N_2 [100–106].

The presence of N defects, which exhibit comparable shapes and sizes to N atoms, can facilitate the selective adsorption and activation of N_2 molecules. At the same time, the incorporation of N defects may enhance the separation efficiency of photogenerated carriers in g-C_3N_4. Consequently, g-C_3N_4 modified with N defects demonstrates superior effectiveness and practicality in photocatalytic nitrogen fixation compared to previously reported photocatalysts. Dong et al. [107] successfully produced N defects-containing g-C_3N_4 for the first time by a secondary calcination process in 2015, which showed excellent performance in photocatalytic nitrogen fixation with a nitrogen fixation rate of 1.24 mmol/(g·h), which is a pioneering work on N defects-containing g-C_3N_4 in photocatalytic nitrogen fixation. Xue et al. [108] employed *in-situ* co-cleavage to synthesize g-C_3N_4 with N_{3C} defects in g-C_3N_4 (g-C_3N_4-N_{3C}). The structural, electronic, and optical characteristics of g-C_3N_4 were specifically modified by N defects engineering strategy to enhance its photocatalytic performance. The optimized g-C_3N_4-N_{3C} showed an optimal photocatalytic N_2 fixation rate of 1915 μmol/(g·h) in the presence of a sacrificial agent, which was 9.5 times higher than that of pure g-C_3N_4. Additionally, it achieved an optimal photocatalytic N_2 fixation rate of 1086 μmol/(g·h), which was 15.5 times higher than that of pure g-C_3N_4. The apparent quantum efficiency (AQE) of the corresponding g-C_3N_4-N_{3C} photocatalysts was evaluated under monochromatic light (λ = 370 nm), which was 7.79% (Figs. 7(a)–7(c)).

The photocatalytic N_2 fixation process is shown in Fig. 7(d). Under simulated sunlight irradiation, g-C_3N_4-N_{3C} was activated to produce photogenerated electrons and holes. The holes oxidized the sacrificial agent, resulting in the formation of oxidation products and protons, while the electrons were captured by the N_{3C} defects

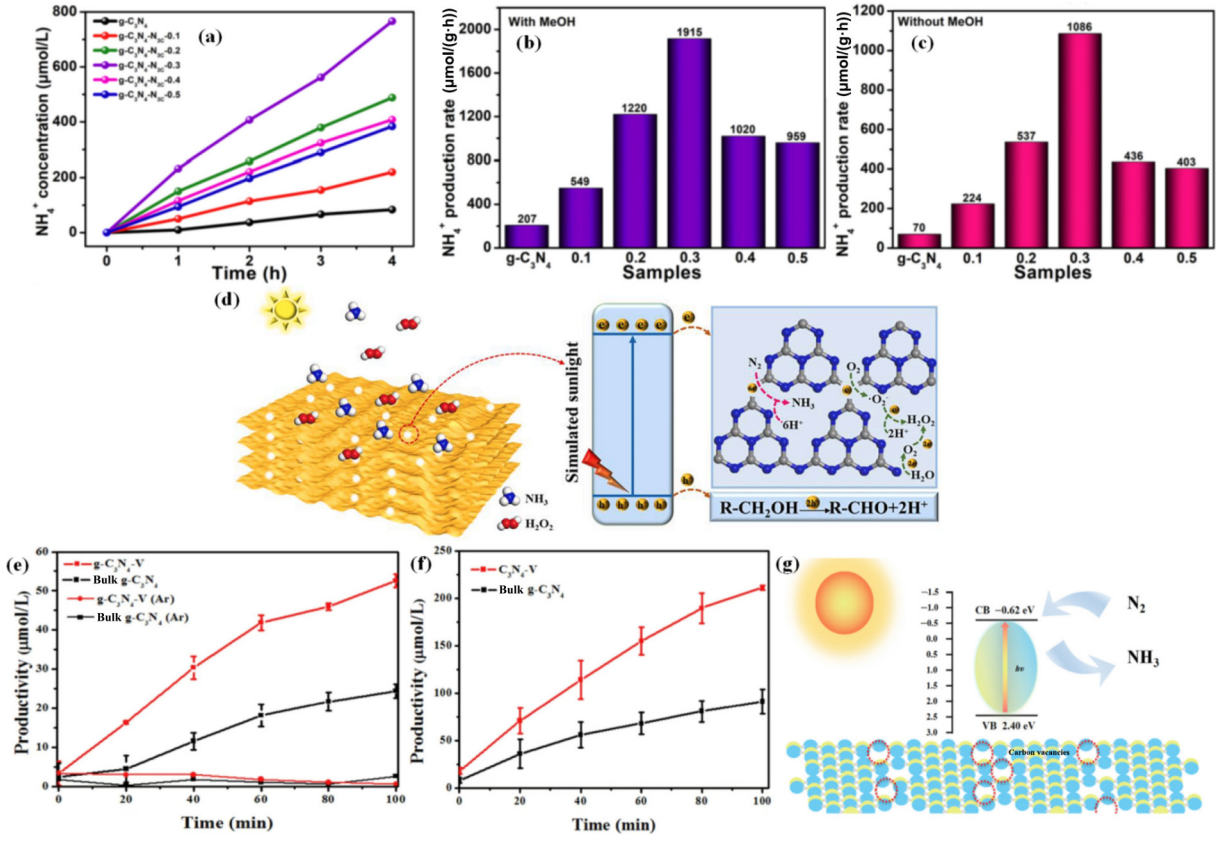

Figure 7 (a) Photocatalytic N_2 fixation of g-C_3N_4 and g-C_3N_4-N_{3C}-*X*; NH^{4+} production rate (b) with MeOH and (c) without MeOH of g-C_3N_4 and g-C_3N_4-N_{3C}-*X*. Reproduced with permission from Ref. [108], © Elsevier B.V. 2022. (d) The proposed mechanism for photocatalytic production of NH_3 and H_2O_2 over g-C_3N_4-N_{3C}; photocatalytic nitrogen fixation over bulk g-C_3N_4 and g-C_3N_4-V materials under light irradiation in (e) pure water and (f) 25% methanol and 75% water. (g) Photocatalytic mechanism diagram of g-C_3N_4-V. Reproduced with permission from Ref. [109], © Elsevier Inc. 2019.

and subsequently transferred to adsorbed N_2 and O_2 molecules, facilitating the reductive reaction with protons in the solution to produce NH_3. Detailed studies showed that the existence of N_{3C} defects had a significant photocatalysis to improve the production of NH_3. Firstly, N_{3C} defects can turn the energy band structure, narrow the band gap, and enhance the light trapping ability. Secondly, N_{3C} defects can act as trap states for photogenerated electrons, promoting the separation and transfer of photogenerated electron and hole pairs. Finally, N_{3C} defects can act as active centers to promote the adsorption and activation of N_2 and O_2 molecules. DFT calculations showed that g-C_3N_4-N_{3C} is more effective at activating N_2 and O_2 molecules compared to pure g-C_3N_4. In summary, the multiple synergistic effects triggered by N defects engineering can improve the photocatalytic performance of g-C_3N_4 photocatalysts.

The introduction of C defects has been shown to significantly enhance nitrogen chemisorption where the C defects can act as electron traps to attract photogenerated electrons. In this way, the trapped electrons are transferred from the C defects to the nitrogen molecule, which activates N_2 to form high-energy intermediates (–N_2H or HN=NH), greatly improving the charge separation efficiency and the photocatalytic N_2 fixation rate. Zhang et al. [109] used a high-temperature exfoliation method to prepare the ultra-thin carbon nitride g-C_3N_4-V (Fig. 7(d)), characterized by its loose and porous with more C defects on the surface. Their findings indicated a substantial enhancement in the photocatalytic activity of g-C_3N_4-V for the conversion of N_2 to NH_3 under visible light, surpassing that of pure g-C_3N_4. Figure 7(e) shows the nitrogen fixation performance of both g-C_3N_4 and g-C_3N_4-V under visible light irradiation. The subsequent experiments conducted in an argon gas atmosphere confirmed that the catalyst insignificantly dissociated elemental nitrogen during the photoreaction. After 100 min of light exposure in the air without the presence of a sacrificial agent, the NH_4^+ produced by g-C_3N_4-V reached 54 mmol/L, which was 2.25 times greater than that generated by pure g-C_3N_4. Furthermore, the NH_4^+ yield from g-C_3N_4-V could be augmented to 212 mmol/L through the addition of a methanol sacrificial agent (Fig. 7(f)). This enhancement was attributed to the thermal exfoliation process, which imparted a loose and porous ultrathin structure to g-C_3N_4-V, thereby significantly increasing its specific surface area and hydrophilicity, which in turn enhanced its nitrogen adsorption capacity. The presence of C defects exposed additional active sites, thereby improving the separation efficiency of photogenerated charge carriers and further augmenting the nitrogen-fixing performance of g-C_3N_4-V (Fig. 7(g)). Additionally, the amino and cyano functional groups formed during defect creation contributed to the improved photocatalytic N_2 fixation activity of g-C_3N_4.

4.6 Photocatalytic disinfection

Waterborne diseases and epidemics caused by pathogens, fungi, viruses, and bacteria pose a great threat to human health and the environment. Traditional disinfection methods often yield mutagenic and carcinogenic by-products, highlighting the necessity

for non-toxic alternatives. In this context, semiconductor photocatalytic disinfection technology pioneered by Matsunaga et al. offers a promising solution, with g-C_3N_4 demonstrated to be effective for microbial sterilization in water [110, 111]. However, the fast carrier complexation rate and small specific surface area can reduce the photocatalytic inhibition efficiency of g-C_3N_4, limiting its application in photocatalytic sterilization. Nevertheless, some research indicates that introducing defects into g-C_3N_4 can create specialized sites for electron trapping, thereby enhancing the separation rate of electron-hole pairs, promoting the generation of reactive species, and significantly improving the efficiency of photocatalytic sterilization [112–114].

In general, photocatalytic bacterial inactivation involves the surface reactions of both photogenerated h^+ and e^-, which can generate reactive oxygen species (ROSs), such as O_2^-, –OH, $^1O_2$, and H_2O_2. It is important to highlight that the surface N defects can act as trapping active centers, and the C adjacent to N defects is more capable of carrying ROSs, thus improving the electron-hole pair separation efficiency and promoting the oxidation of photocatalytically active substances, which provides more adsorption sites for the reaction, and directly accelerates bacterial death. Zhong et al. [115] utilized a rapid thermal stripping and thermal polymerization method to synthesize N-deficient ultrathin g-C_3N_4 nanosheets (DUCN-500), which demonstrated remarkable bactericidal efficacy. Specifically, DUCN-500 achieved complete deactivation of *E. coli* at a concentration of 7.0 $\log_{10}$CFU/mL within 60 min (Fig. 8(a)) and successfully deactivated *Bacillus subtilis* at a concentration of 7.1 $\log_{10}$CFU/mL in 75 min (Fig. 8(b)). Furthermore, the study confirmed that DUCN-500 exhibited significant anticorrosive properties and stability in real water systems. The presence of N defects within the catalyst facilitated carrier separation, accelerated charge transport, and generated more $\cdot O_2^-$ and H_2O_2 by about 4.6-fold, which was attributed to the negative shift of the conduction band potential and rapid separation of charge carriers. Additionally, the ultrathin nanosheet structure effectively reduced the energy barrier, promoting closer interaction between the bacteria and the photocatalyst, thereby significantly improving the bacterial trapping efficiency of g-C_3N_4 and enhancing the utilization of reactive oxygen species. The reactive oxygen species induced morphological damage to the bacteria, diminished antioxidant enzyme activity, and caused protein leakage, ultimately resulting in bacterial mortality (Fig. 8(c)). Similarly, Liu et al. [116] prepared porous ultrathin g-C_3N_4 nanosheets (CN) with N defects by the thermal polymerization of freeze-dried HCl-pretreated urea precursors. DFT calculations demonstrated the successful introduction of N defects in the triazine unit of g-C_3N_4, which was further substantiated by EPR, XPS, photoluminescence (PL), and time-resolved PL (TR-PL). The delocalization of lone-pair electrons associated with these defects was shown to enhance the π-conjugated covalent system and the catalytic activity of CN-4. UV–vis diffuse reflectance spectra (DRS), PL, TR-PL, IT, and EIS indicated that CN-4 exhibited improved visible light absorption, a greater number of exposed active sites, enhanced mass and charge transfer rates, and increased efficiencies in the separation of photo-induced electrons and holes (Fig. 8(d)). EPR, trap agent experiments, and spectral semiquantitative experiments revealed that holes (h^+) and superoxide anions ($\cdot O_2^-$) play a significant role in the photocatalytic inhibition of *E. coli.* (Fig. 8(e)). In comparison to CN, the optimized CN-4 demonstrated superior efficacy in inhibiting *E. coli* and *S. aureus* after 120 min of photocatalytic treatment, resulting in bacterial colony reductions of 4.80 and 4.24 $\log_{10}$CFU/mL, respectively (Fig. 8(f)). Different mechanisms of cellular damage were indicated for *E. coli* and *S. aureus* by SEM (Figs. 8(g) and 8(h)), where photocatalytic generation of reactive free radicals led to the oxidative rupture of *E. coli* cell membranes leading to eventual death, while physical adsorption and mechanical binding impaired the activity of *S. aureus* cell membranes, ultimately resulting in cell death.

Based on the results in the literature, the bacterial inhibition effect of individual C defect is less significant. This may be attributed to the positive charge C defects, in contrast to the negatively charged or neutral nature of C defects, which is unfavorable to the adsorption of *E. coli.* Consequently, it is essential to augment photocatalytic activity by integrating C defects with other materials, such as through the doping of non-metallic elements. Dahlan et al. [117] revealed the photocatalytic inactivation of *E. coli* cells by ultrathin oxygen-doped g-C_3N_4 nanosheets with carbon defects (OCvN) via facile gas bubble template-assisted thermal copolymerization method. In the evaluation of photocatalytic inactivation of *E. coli*, OCvN-3 exhibited remarkable disinfection efficacy, achieving a reduction of over 7 logs (> 99.99999%) after three hours of illumination, which represented an 18-fold enhancement in antibacterial activity relative to that of pristine g-C_3N_4. The superior efficacy was attributed to the synergistic effects of extended light response, improved electronic conductivity, and significantly reduced resistance to charge transfer.

4.7 H_2O_2 production

H_2O_2 is widely used as a potential clean and high-energy oxidant in many fields such as chemical synthesis, sterilization, wastewater treatment, paper bleaching, and fuel cells. However, the traditional H_2O_2 production methods have severe shortcomings, such as highly energy-consuming or complex industrial processes and high production costs [118–120]. In recent years, the semiconductor material represented by g-C_3N_4 has been considered as one of the promising technologies to realize safe, green, and sustainable synthesis of H_2O_2 by using solar energy to drive the conversion of water and oxygen into H_2O_2. However, the disadvantages of g-C_3N_4 such as weak visible light absorption, slow photogenerated electron-hole pair separation, and limited adsorption energy of O_2 affect its reactivity thus limiting its practical application. The introduction of defects into the g-C_3N_4 structure has been embraced as an efficient technique for considerably increasing photocatalytic activity. Since the defect created in g-C_3N_4 can reduce the symmetry of g-C_3N_4 and narrow the band gap, it allows to increase the number of excitable electrons and enhance the visible light absorption range. Meanwhile, the vacancy defects, due to the abundance of localized electrons, can improve the adsorption and activation ability of g-C_3N_4 for O_2. Therefore, the modification of g-C_3N_4 with intrinsic defects is conducive to improving the efficiency of H_2O_2 photocatalytic production [121–124]. Shi et al. [125] synthesized porous g-C_3N_4 (DCN) containing N defects via a novel photoassisted heating process. The results illustrated in Figs. 9(a)–9(c) demonstrate that the photoassisted treatment and the incorporation of N defects resulted in substantial alterations to the morphology and electronic structure of g-C_3N_4. These modifications subsequently enhanced the photocatalytic efficacy of DCN, where the formation of abundant holes endowed more catalytically active sites and transplanar diffusion channels,

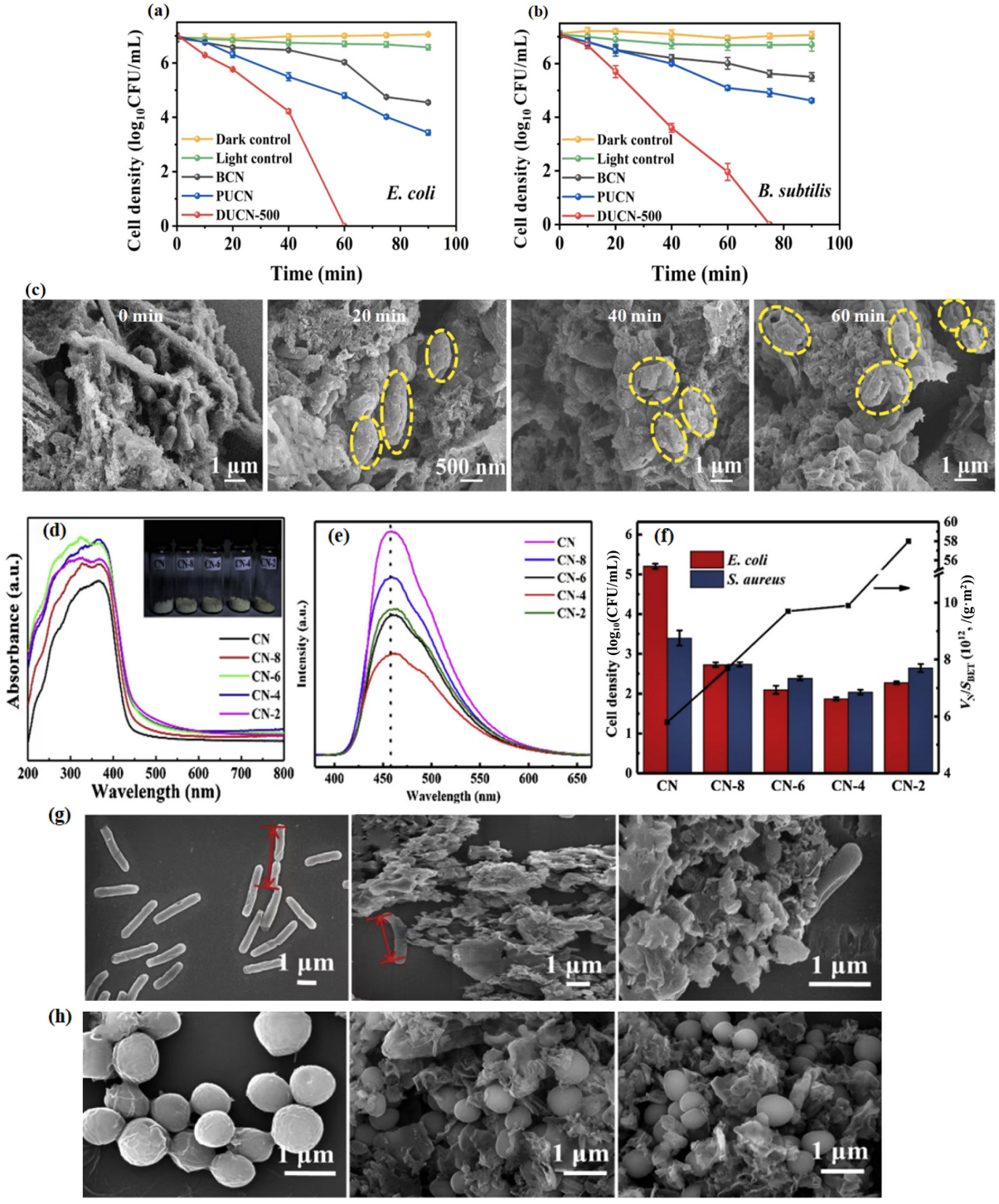

Figure 8 Photocatalytic inactivation efficiencies toward (a) *E. coli* and (b) *B. subtilis* using as-synthesized photocatalysts; (c) photographs of *E. coli* at different phases of photocatalytic inactivation; SEM images of *E. coli* after photocatalytic treatment with DUCN-500 (at 0, 20, 40, and 60 min). Reproduced with permission from Ref. [115], © Zhong, K. Q. et al. 2023. (d) UV–vis diffuse reflection spectra (the inset are graphs of all CN samples); (e) photoluminescence spectra (excited at 370 nm); (f) the inactivation efficiency and VN/SBET of samples; SEM images of *E. coli* (g) and *S. aureus* (h) treated with CN-4 (100 mg/L) under visible light at 0, 30, and 60 min. Reproduced with permission from Ref. [116], © Elsevier B.V. 2019.

shortening the diffusion distance of reactants from the surface to the bulk and charge carriers from the bulk to the surface. The introduction of N defects resulted in narrowing a smaller intrinsic bandgap, extending the visible-light absorption range, and suppressing the radiative electron–hole recombination, which significantly enhanced the photocatalytic activity of H_2O_2 production. Figure 9(d) shows the time-dependent evolution of H_2O_2 produced by BCN and DCN samples. The concentration of H_2O_2 increased almost linearly as irradiation time prolongs, indicating that all the samples can produce H_2O_2 in the photocatalytic reaction system. After photocatalytic reaction for 2.5 h, about 12.1 μmol of H_2O_2 was produced on DCN-15A, which

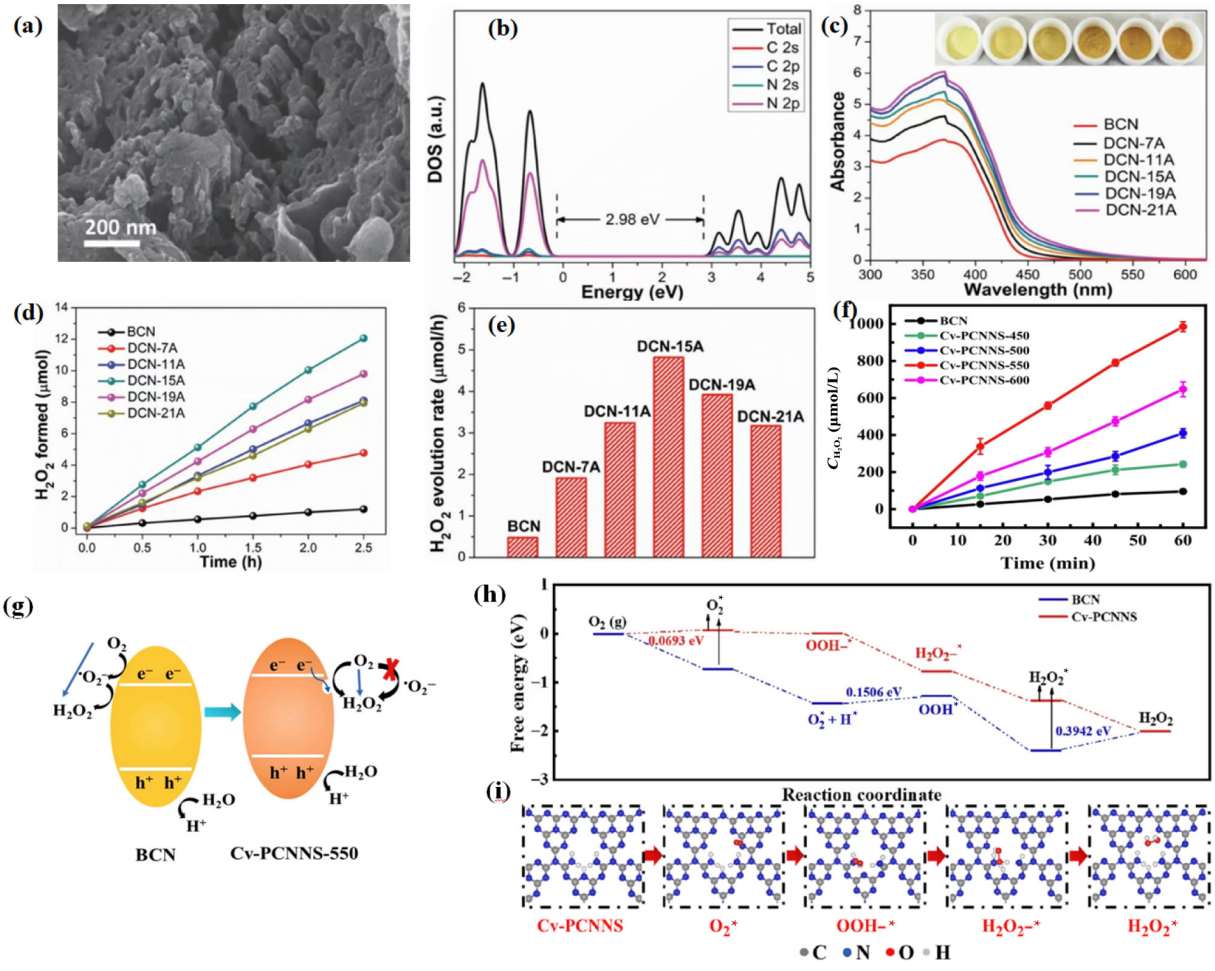

Figure 9 (a) SEM image of DCN-15A; (b) density of states of DCN; (c) UV–vis absorption spectraand corresponding pictures of BCN and DCN samples; (d) time-dependent evolution of H_2O_2 produced by BCN and DCN samples; (e) photocatalytic H_2O_2 activity comparison of different samples. Reproduced with permission from Ref. [125], © WILEY-VCH Verlag GmbH & Co. KGaA, Weinheim 2018. (f) Photocatalytic H_2O_2 with BCN and Cv-PCNNS prepared under different temperatures; (g) corresponding mechanism for photocatalytic H_2O_2 production based on BCN and Cv-PCNNS-550; (h) free-energy diagrams for the reduction of O_2 to H_2O_2 on BCN and Cv-PCNNS; (i) corresponding optimized geometries for the reduction of O_2 into H_2O_2 on Cv-PCNNS. Reproduced with permission from Ref. [127], © Elsevier B.V. 2023.

was 10.1 times more than that of the pristine g-C_3N_4 (Fig. 9(e)). The synergistic effect of N defects with other functional group defects can also enhance the g-C_3N_4 photocatalytic synthesis of H_2O_2. Li et al. [126] prepared g-C_3N_4 with abundant N defects and cyano groups (Nv-M) by high temperature calcination of bulk g-C_3N_4 in the presence of KOH. The Nv-M exhibited a remarkable H_2O_2 generation rate of 623.5 μmol/(g·h), which was about 7 times higher than that of pristine g-C_3N_4. The introduction of N defects and cyano groups enhanced visible light absorption, facilitated carrier transport, and effectively reduced carrier recombination. Additionally, the presence of surface reactive oxygen adsorption sites fostered the generation of O_2^- and $^1O_2$, and promoted selective $2e^-$ oxygen reduction reaction (ORR) and oxidized water generation of O_2.

Similar to N defects, C defects also have shown excellent performance in enhancing the photocatalytic H_2O_2 production efficiency of g-C_3N_4. For example, Li et al. [127] prepared porous g-C_3N_4 nanosheets with C defects (Cv-PCNNS) by the thermal polymerization of urea and subsequent heat treatment under Ar atmosphere. The incorporation of C defects in CvP-PCNNS resulted in a reduction of the symmetry of g-C_3N_4, facilitating electron delocalization. This modification led to an increase in the number of excited electrons and a reduction in the band gap of g-C_3N_4, thereby enhancing both photo-induced charge separation and oxygen activation. Under optimal conditions, Cv-PCNNS-550 achieved a higher H_2O_2 production of 984.8 μmol/(L·h), which was 10 times higher than that of pristine g-C_3N_4 (Fig. 9(f)). It is generally believed that H_2O_2 can be produced via either two-step single-electron reduction pathway ($O_2 \rightarrow O_2^- \rightarrow H_2O_2$) or a one-step dual-electron reduction ($O_2 \rightarrow H_2O_2$) reaction. By trapping active species with rotating disc electrodes (RDEs), the introduction of C defects led to the transformation of ORR from a two-step single-electron reduction process to a one-step two-electron direct reduction process, thereby accelerating the H_2O_2 production. The proposed reaction mechanism for the photocatalytic H_2O_2 production using Cv-PCNNS is illustrated (Fig. 9(g)). The reaction pathways for the H_2O_2 production of g-C_3N_4 and Cv-PCNNS were also investigated by DFT, and the results are shown in Fig. 9(h). The g-C_3N_4 reduction step (blue line) consists of the following steps: (1) O_2 molecules are adsorbed on g-C_3N_4 to generate O_2*; (2) reactive H atoms are adsorbed to form H*; (3) O_2* combined with an H* to generate *OOH; (4) *OOH species captured another H* to

generate H_2O_2*; and (5) H_2O_2* is desorbed to generate H_2O_2. The red line in Fig. 9(g) shows the free energy of H_2O_2 synthesis by Cv-PCNNS, and Fig. 9(i) shows the simulation of the reaction process of O_2 reduction to generate H_2O_2 on Cv-PCNNS.

5 Conclusions

In summary, the introduction of different defects can effectively change the electronic band structure of g-C_3N_4, delay carrier recombination, and increase the surface reactive sites to acquire an ameliorated photocatalytic activity. In this review, the current research and applications of intrinsically defective g-C_3N_4-based materials are comprehensively reviewed, and the relationship between the structure and properties of g-C_3N_4-based materials is thoroughly examined. Firstly, different types of intrinsic defects in g-C_3N_4 are discussed and their modification strategies are analyzed. Intrinsic defects are classified into two main types: vacancy defects and reactive defects. Vacancy defects contain C, N, amino, and cyano functional groups, whereas reactive defects include C and N self-doping. The positioning of these defects can be precisely controlled through various methods, such as calcination, hydrothermal/solvent-thermal methods, molten salt heat treatment, chemical reduction, gas etching, and acid /alkali etching. Different modification strategies can generate different effects, the introduction of intrinsic defects can enhance light absorption, facilitate rapid charge transfer, and promote efficient surface reactions. Moreover, defects often serve as reservoirs for photoinduced electrons, facilitating charge separation and trapping sites to transfer captured photoexcited electrons to dissociated O_2, generating reactive oxygen species, and promoting the redox capability. In addition, the applications of intrinsic defect-type g-C_3N_4-based materials in diverse photocatalytic fields are summarized elaborately, including wastewater remediation, hydrogen evolution, CO_2 conversion, NO removal, nitrogen fixation, photocatalytic disinfection, and H_2O_2 production. In particular, the representative work on defect-engineered g-C_3N_4 in various environmental remediation, clean energy production, and catalytic processes in recent years is outlined.

Despite the significant advantages of defect-type g-C_3N_4-based materials and their broad application prospects, there are still some challenges in their design, synthesis, and, which are specifically as follows.

(1) Innovate and develope environmentally friendly defect modulation strategies. g-C_3N_4-based photocatalytic materials have been applied in various photocatalytic fields, while most of g-C_3N_4-based materials are only limited for some specific applications. It is worth to note that the current research progress is still far from meeting the practical application needs. In addition, traditional defect modulation methods mainly rely on strong acids or bases to accelerate the formation of defects. Future research may focus on designing highly efficienct, controllable treatment with low cost in the synthesis of vacancy defect modification g-C_3N_4, by improved methods such as microwaves assisted and hydrothermal processes.

(2) Accurately identifying and quantifying defects in g-C_3N_4 remains a challenging task using the current material characterization methods. The main issue is related to establishing a structure–activity relationship between the properties of photocatalysts and the known extent of defects, largely due to the low resolution of current characterization techniques. Thus, it is necessary to employ more advanced techniques such as optical (e.g., fs-femtosecond transient absorption spectroscopy) and electrochemical method (EIS analysis).

(3) Defect stability is still a big challenge in the practical implementation. Due to the long-term solar irradiation, the more inert bulk g-C_3N_4 material inevitably experiences degradation of its photocatalytic activity. The defects, dopants, functional groups, and single/dual atoms may undergo more complex structural changes. Furthermore, there is currently a lack of insights into the structural evolution of defects during the catalytic process. Therefore, more advanced real-time analysis technologies and effective process strategies are needed to detect and stabilize these defective g-C_3N_4.

(4) Despite various defect modulation strategies of g-C_3N_4 being proposed, the in-depth understanding of the mechanism of different systems is still poor. There are many unknowns to be further investigated, such as the intimate relationship between the defects types of g-C_3N_4 and the key factors in the photocatalysis, and the functions of various defects in other steps during the photocatalytic process. All these challenges need to be addressed through thorough studies in conjunction with advanced technologies, such as theoretical analysis and *in-situ* characterization.

Data availability

All data needed to support the conclusions in the paper are presented in the manuscript. Additional data related to this paper may be requested from the corresponding author upon request.

Acknowledgements

This work was supported by the Key Research and Development Program of Shaanxi Province (No. 2022ZDLSF07-04), Xi'an Science and Technology Projects (Nos. 2022JH-RYFW-0114 and 2023JH-GXRC-0196), and Graduate Innovation Fund Project of Xi'an Shiyou University (No. YCX2411003).

Declaration of competing interest

All the contributing authors report no conflict of interests in this work.

Author contribution statement

S. C. W.: Acquisition, data curation, writing manuscript, investigation. L. T. W.: Acquisition, data curation, investigation. W. L.: Writing manuscript, visualization. M. L.: Writing manuscript, data curation. C. Y. K.: Supervision, project administration, funding. J. F. H.: Supervision, resources, administration.

Use of AI statement

None.

References

[1] Cao, S. W.; Low, J. X.; Yu, J. G.; Jaroniec, M. Polymeric photocatalysts based on graphitic carbon nitride. *Adv. Mater.* **2015**, *27*, 2150–2176.

[2] Debnath, K. B.; Mourshed, M. Challenges and gaps for energy planning models in the developing-world context. *Nat. Energy* **2018**, *3*, 172–184.

[3] Kittner, N.; Lill, F.; Kammen, D. M. Energy storage deployment and

innovation for the clean energy transition. *Nat. Energy* **2017**, *2*, 17125.
[4] Lewis, N. S. Research opportunities to advance solar energy utilization. *Science* **2016**, *351*, aad1920.
[5] Cortright, R. D.; Davda, R. R.; Dumesic, J. A. Hydrogen from catalytic reforming of biomass-derived hydrocarbons in liquid water. *Nature* **2002**, *418*, 964–967.
[6] Xiong, J.; Di, J.; Xia, J. X.; Zhu, W. S.; Li, H. M. Surface defect engineering in 2D nanomaterials for photocatalysis. *Adv. Funct. Mater.* **2018**, *28*, 1801983.
[7] Song, X. L.; Chen, L.; Gao, L. J.; Ren, J. T.; Yuan, Z. Y. Engineering g-C_3N_4 based materials for advanced photocatalysis: Recent advances. *Green Energy Environ.* **2022**, *9*, 166–197.
[8] Wang, Y. H.; Liu, L. Z.; Ma, T. Y.; Zhang, Y. H.; Huang, H. W. 2D graphitic carbon nitride for energy conversion and storage. *Adv. Funct. Mater.* **2021**, *31*, 2102540.
[9] Zhang, M. L.; Yang, Y.; An, X. Q.; Hou, L. A. A critical review of g-C_3N_4-based photocatalytic membrane for water purification. *Chem. Eng. J.* **2021**, *412*, 128663.
[10] Zhan, H. Y.; Zhou, R. R.; Liu, K. W.; Ma, Z. H.; Wang, P. F.; Zhan, S. H.; Zhou, Q. X. Progress and challenges of photocatalytic reduction of CO_2 with g-C_3N_4-based photocatalysts in the context of carbon neutrality. *Sci. China Mater.* **2024**, *67*, 1740–1764.
[11] Ajmal, Z.; Haq, M. U.; Naciri, Y.; Djellabi, R.; Hassan, N.; Zaman, S.; Murtaza, A.; Kumar, A.; Al-Sehemi, A. G.; Algarni, H. et al. Recent advancement in conjugated polymers based photocatalytic technology for air pollutants abatement: Cases of CO_2, NO_x, and VOCs. *Chemosphere* **2022**, *308*, 136358.
[12] Barrio, J.; Volokh, M.; Shalom, M. Polymeric carbon nitrides and related metal-free materials for energy and environmental applications. *J. Mater. Chem. A* **2020**, *8*, 11075–11116.
[13] Xing, Y. P.; Wang, X. K.; Hao, S. H.; Zhang, X. L.; Wang, X.; Ma, W. X.; Zhao, G.; Xu, X. J. Recent advances in the improvement of g-C_3N_4 based photocatalytic materials. *Chin. Chem. Lett.* **2021**, *32*, 13–20.
[14] Cai, M.; Wei, Y. X.; Li, Y. K.; Li, X.; Wang, S. B.; Shao, G. S.; Zhang, P. 2D semiconductor nanosheets for solar photocatalysis. *EcoEnergy* **2023**, *1*, 248–295.
[15] Teixeira, I. F.; Barbosa, E. C. M.; Tsang, S. C. E.; Camargo, P. H. C. Carbon nitrides and metal nanoparticles: From controlled synthesis to design principles for improved photocatalysis. *Chem. Soc. Rev.* **2018**, *47*, 7783–7817.
[16] Tian, N.; Huang, H. W.; Du, X.; Dong, F.; Zhang, Y. H. Rational nanostructure design of graphitic carbon nitride for photocatalytic applications. *J. Mater. Chem. A* **2019**, *7*, 11584–11612.
[17] Kavitha, R.; Nithya, P. M.; Girish Kumar, S. Noble metal deposited graphitic carbon nitride based heterojunction photocatalysts. *Appl. Surf. Sci.* **2020**, *508*, 145142.
[18] Wan, C.; Zhou, L.; Xu, S. M.; Jin, B. Y.; Ge, X.; Qian, X.; Xu, L. X.; Chen, F. Q.; Zhan, X. L.; Yang, Y. R. et al. Defect engineered mesoporous graphitic carbon nitride modified with AgPd nanoparticles for enhanced photocatalytic hydrogen evolution from formic acid. *Chem. Eng. J.* **2022**, *429*, 132388.
[19] Yang, J. J.; Wang, H.; Jiang, L. B.; Yu, H. B.; Zhao, Y. L.; Chen, H. Y.; Yuan, X. Z.; Liang, J.; Li, H.; Wu, Z. B. Defective polymeric carbon nitride: Fabrications, photocatalytic applications and perspectives. *Chem. Eng. J.* **2022**, *427*, 130991.
[20] Maarisetty, D.; Baral, S. S. Defect engineering in photocatalysis: Formation, chemistry, optoelectronics, and interface studies. *J. Mater. Chem. A* **2020**, *8*, 18560–18604.
[21] Li, Y. H.; He, Z. J.; Liu, L.; Jiang, Y.; Ong, W. J.; Duan, Y. Y.; Ho, W. K.; Dong, F. Inside-and-out modification of graphitic carbon nitride (g-C_3N_4) photocatalysts via defect engineering for energy and environmental science. *Nano Energy* **2023**, *105*, 108032.
[22] Bai, S.; Zhang, N.; Gao, C.; Xiong, Y. J. Defect engineering in photocatalytic materials. *Nano Energy* **2018**, *53*, 296–336.
[23] Xu, Y. S.; Fan, M. J.; Yang, W. J.; Xiao, Y. H.; Zeng, L. T.; Wu, X.; Xu, Q. H.; Su, C. L.; He, Q. J. Homogeneous carbon/potassium-incorporation strategy for synthesizing red polymeric carbon nitride capable of near-infrared photocatalytic H_2 production. *Adv. Mater.* **2021**, *33*, 2101455.
[24] Corp, K. L.; Schlenker, C. W. Ultrafast spectroscopy reveals electron-transfer cascade that improves hydrogen evolution with carbon nitride photocatalysts. *J. Am. Chem. Soc.* **2017**, *139*, 7904–7912.
[25] Jiang, L. B.; Yang, J. J.; Yuan, X. Z.; Guo, J. Y.; Liang, J.; Tang, W. W.; Chen, Y. N.; Li, X. D.; Wang, H.; Chu, W. Defect engineering in polymeric carbon nitride photocatalyst: Synthesis, properties and characterizations. *Adv. Colloid Interface Sci.* **2021**, *296*, 102523.
[26] Luo, L.; Wang, K. R.; Gong, Z. Y.; Zhu, H. X.; Ma, J. N.; Xiong, L. Q.; Tang, J. W. Bridging-nitrogen defects modified graphitic carbon nitride nanosheet for boosted photocatalytic hydrogen production. *Int. J. Hydrogen Energy* **2021**, *46*, 27014–27025.
[27] Xie, C.; Yan, D. F.; Li, H.; Du, S. Q.; Chen, W.; Wang, Y. Y.; Zou, Y. Q.; Chen, R.; Wang, S. Y. Defect chemistry in heterogeneous catalysis: Recognition, understanding, and utilization. *ACS Catal.* **2020**, *10*, 11082–11098.
[28] Hou, S. Q.; Gao, X. C.; Lv, X. Y.; Zhao, Y. L.; Yin, X. T.; Liu, Y.; Fang, J.; Yu, X. X.; Ma, X. G.; Ma, T. Y. et al. Decade milestone advancement of defect-engineered g-C_3N_4 for solar catalytic applications. *Nano-Micro Lett.* **2024**, *16*, 70.
[29] Wang, G. L.; Zhao, Y.; Ma, H. R.; Zhang, C. J.; Dong, X. L.; Zhang, X. F. Enhanced peroxymonosulfate activation on dual active sites of N vacancy modified g-C_3N_4 under visible-light assistance and its selective removal of organic pollutants. *Sci. Total Environ.* **2021**, *756*, 144139.
[30] Jiao, S. L.; Fu, X. W.; Zhang, L.; Zeng, Y. J.; Huang, H. W. Point-defect-optimized electron distribution for enhanced electrocatalysis: Towards the perfection of the imperfections. *Nano Today* **2020**, *31*, 100833.
[31] Niu, P.; Yin, L. C.; Yang, Y. Q.; Liu, G.; Cheng, H. M. Increasing the visible light absorption of graphitic carbon nitride (melon) photocatalysts by homogeneous self-modification with nitrogen vacancies. *Adv. Mater.* **2014**, *26*, 8046–8052.
[32] Guo, F.; Wang, L. J.; Sun, H. R.; Li, M. Y.; Shi, W. L.; Lin, X. A one-pot sealed ammonia self-etching strategy to synthesis of N-defective g-C_3N_4 for enhanced visible-light photocatalytic hydrogen. *Int. J. Hydrogen Energy* **2020**, *45*, 30521–30532.
[33] Zhao, C.; Shi, C. J.; Li, Q.; Wang, X. Y.; Zeng, G.; Ye, S.; Jiang, B. J.; Liu, J. Nitrogen vacancy-rich porous carbon nitride nanosheets for efficient photocatalytic H_2O_2 production. *Mater. Today Energy* **2022**, *24*, 100926.
[34] Tan, J.; Tian, N.; Li, Z. F.; Li, J.; Yao, X. L.; Vakili, M.; Lu, Y.; Zhang, T. T. Intrinsic defect engineering in graphitic carbon nitride for photocatalytic environmental purification: A review to fill existing knowledge gaps. *Chem. Eng. J.* **2021**, *421*, 127729.
[35] Shen, M.; Zhang, L. X.; Wang, M.; Tian, J. J.; Jin, X. X.; Guo, L. M.; Wang, L. Z.; Shi, J. L. Carbon-vacancy modified graphitic carbon nitride: enhanced CO_2 photocatalytic reduction performance and mechanism probing. *J. Mater. Chem. A.* **2019**, *7*, 1556–1563.
[36] Liang, Q. H.; Li, Z.; Huang, Z. H.; Kang, F. Y.; Yang, Q. H. Holey graphitic carbon nitride nanosheets with carbon vacancies for highly improved photocatalytic hydrogen production. *Adv. Funct. Mater.* **2015**, *25*, 6885–6892.
[37] Gao, S. Y.; Wang, X. Y.; Song, C. J.; Zhou, S. J.; Yang, F.; Kong, Y. Engineering carbon-defects on ultrathin g-C_3N_4 allows one-pot output and dramatically boosts photoredox catalytic activity. *Appl. Catal. B: Environ.* **2021**, *295*, 120272.
[38] Iqbal, O.; Ali, H.; Li, N.; Al-Sulami, A. I.; Alshammari, K. F.; Abd-Rabboh, H. S. M.; Al-Hadeethi, Y.; Din, I. U.; Alharthi, A. I.; Altamimi, R. et al. A review on the synthesis, properties, and characterizations of graphitic carbon nitride (g-C_3N_4) for energy

conversion and storage applications. *Mater. Today Phys.* **2023**, *34*, 101080.

[39] Lau, V. W. H.; Moudrakovski, I.; Botari, T.; Weinberger, S.; Mesch, M. B.; Duppel, V.; Senker, J.; Blum, V.; Lotsch, B. V. Rational design of carbon nitride photocatalysts by identification of cyanamide defects as catalytically relevant sites. *Nat. Commun.* **2016**, *7*, 12165.

[40] Tan, H.; Gu, X. M.; Kong, P.; Lian, Z.; Li, B.; Zheng, Z. F. Cyano group modified carbon nitride with enhanced photoactivity for selective oxidation of benzylamine. *Appl. Catal. B: Environ.* **2019**, *242*, 67–75.

[41] Zhao, B. B.; Xu, J. C.; Liu, Y. P.; Fan, J. J.; Yu, H. G. Amino group-rich porous g-C_3N_4 nanosheet photocatalyst: Facile oxalic acid-induced synthesis and improved H_2-evolution activity. *Ceram. Int.* **2021**, *47*, 18295–18303.

[42] Niu, P.; Qiao, M.; Li, Y. F.; Huang, L.; Zhai, T. Y. Distinctive defects engineering in graphitic carbon nitride for greatly extended visible light photocatalytic hydrogen evolution. *Nano Energy* **2018**, *44*, 73–81.

[43] Ma, H. X.; Jia, Y. F.; Zhu, G. Q.; Zhang, F. C.; Rhee, S.; Lee, B.; Liu, C. L. Study of cyano and hydroxyl groups modification on the properties of porous carbon nitride synthesized by using a salt assistant method. *Appl. Surf. Sci.* **2020**, *507*, 144885.

[44] Li, H. L.; Li, F. P.; Wang, Z. Y., Jiao, Y. C.; Liu, Y. Y.; Wang, P.; Zhang, X. Y.; Qin, X. Y.; Dai, Y.; Huang, B. B. Fabrication of carbon bridged g-C3N4 through supramolecular self-assembly for enhanced photocatalytic hydrogen evolution. *Appl. Catal. B: Environ.* **2018**, *229*, 114–120.

[45] Bao, N.; Hu, X. D.; Zhang, Q. Z.; Miao, X. H.; Jie, X. Y.; Zhou, S. Synthesis of porous carbon-doped g-C_3N_4 nanosheets with enhanced visible-light photocatalytic activity. *Appl. Surf. Sci.* **2017**, *403*, 682–690.

[46] Wang, X. Y.; Sang, L. B.; Zhang, L.; Yang, G.; Guo, Y. H.; Yang, Y. X. Controllable synthesis for carbon self-doping and structural defect co-modified g-C_3N_4: Enhanced photocatalytic oxidation performance and the mechanism insight. *J. Alloys Compd.* **2023**, *941*, 168921.

[47] Xing, J. N.; Huang, X.; Yong, X.; Li, X.; Li, J.; Wang, J. K.; Wang, N.; Hao, H. X. N-doped synergistic porous thin-walled g-C_3N_4 nanotubes for efficient tetracycline photodegradation. *Chem. Eng. J.* **2023**, *455*, 140570.

[48] Zhu, Y. T.; Yuan, D. D.; Zhang, H.; Xu, T.; Sun, L. T. Atomic-scale insights into the formation of 2D crystals from *in situ* transmission electron microscopy. *Nano Res.* **2021**, *14*, 1650–1658.

[49] Lin, B.; Yang, G. D.; Wang, L. Z. Stacking-layer-number dependence of water adsorption in 3D ordered close-packed g-C_3N_4 nanosphere arrays for photocatalytic hydrogen evolution. *Angew. Chem., Int. Ed.* **2019**, *58*, 4587–4591.

[50] Zhan, B. B.; Hao, Y. L.; Qi, X. S.; Qu, Y. P.; Ding, J. F.; Yang, J. L.; Gong, X.; Chen, Y. L.; Peng, Q.; Zhong, W. Multifunctional cellular carbon foams derived from chitosan toward self-cleaning, thermal insulation, and highly efficient microwave absorption properties. *Nano Res.* **2024**, *17*, 927–938.

[51] Whitehead, C. B.; Finke, R. G. Particle formation mechanisms supported by *in situ* synchrotron XAFS and SAXS studies: A review of metal, metal-oxide, semiconductor and selected other nanoparticle formation reactions. *Mate. Adv.* **2021**, *2*, 6532–6568.

[52] Yang, P. J.; Zhuzhang, H. Y.; Wang, R. R.; Lin, W.; Wang, X. C. Carbon vacancies in a melon polymeric matrix promote photocatalytic carbon dioxide conversion. *Angew. Chem., Int. Ed.* **2019**, *58*, 1134–1137.

[53] Zhao, D. M.; Dong, C. L.; Wang, B.; Chen, C.; Huang, Y. C.; Diao, Z. D.; Li, S. Z.; Guo, L. J.; Shen, S. H. Synergy of dopants and defects in graphitic carbon nitride with exceptionally modulated band structures for efficient photocatalytic oxygen evolution. *Adv. Mater.* **2019**, *31*, 1903545.

[54] Guo, L. P.; Gao, J. Y.; Li, M. X.; Xie, Y.; Chen, H.; Wang, S. J.; Li, Z. Z.; Wang, X. P.; Zhou, W. Synergy of defect engineering and curvature effect for porous graphite carbon nitride nanotubes promoted photocatalytic hydrogen evolution. *EcoEnergy* **2023**, *1*, 437–447.

[55] Shen, H. D.; Zhan, X. Y.; Hong, S.; Xu, L.; Yang, C. M.; Robertson, A. W.; Hao, L. D.; Fu, F.; Sun, Z. Y. Ultrafine MoO_x clusters anchored on g-C_3N_4 with nitrogen/oxygen dual defects for synergistic efficient O_2 activation and tetracycline photodegradation. *Nano Res.* **2023**, *16*, 10713–10723.

[56] Preeyanghaa, M.; Erakulan, E. S.; Thapa, R.; Ashokkumar, M.; Neppolian, B. Scrutinizing the role of tunable carbon vacancies in g-C_3N_4 nanosheets for efficient sonophotocatalytic degradation of Tetracycline in diverse water matrices: Experimental study and theoretical calculation. *Chem. Eng. J.* **2023**, *452*, 139437.

[57] Song, P.; Du, J.; Ma, X. L.; Shi, Y. M.; Fang, X. Y.; Liu, D. B.; Wei, S. Q.; Liu, Z. F.; Cao, Y. Y.; Lin, B. et al. Design of $Bi_4O_5Br_2$/g-C_3N_4 heterojunction for efficient photocatalytic removal of persistent organic pollutants from water. *EcoEnergy* **2023**, *1*, 197–206.

[58] Fan, E. C.; Xu, H. L.; Sun, S. P.; Huang, C. N.; Li, M. L.; Fan, B. B.; Shao, G.; Liu, W.; Wang, H. L.; Lu, H. X. et al. Significant enhancement of photocatalytic activity of g-C_3N_4/vermiculite composite by the introduction of nitrogen defects. *Colloids Surf. A* **2023**, *669*, 131510.

[59] Liang, X. F.; Wang, G. L.; Dong, X. L.; Wang, G. W.; Ma, H. C.; Zhang, X. F. Graphitic carbon nitride with carbon vacancies for photocatalytic degradation of bisphenol A. *ACS Appl. Nano Mater.* **2019**, *2*, 517–524.

[60] Li, Y. W.; Zhang, Z. F.; Li, S. Z.; Liu, L. Y.; Ma, W. L. Solar-induced efficient propylparaben photodegradation by nitrogen vacancy engineered reticulate g-C_3N_4: Morphology, activity and mechanism. *Sci. Total Environ.* **2023**, *856*, 159247.

[61] Zhang, Z.; Zheng, Y. M.; Xie, H.; Zhao, J. J.; Guo, X. L.; Zhang, W. J.; Fu, Q. P.; Wang, S. H.; Xu, Q.; Huang, Y. Synthesis of g-C_3N_4 microrods with superficial C, N dual vacancies for enhanced photocatalytic organic pollutant removal and H_2O_2 production. *J. Alloys Compd.* **2022**, *904*, 164028.

[62] Guo, Y. J.; Liu, G.; Yin, W. H.; Zhang, Y. S.; Shi, L. Precise defect engineering g-C_3N_4 fabrication to improve hydrogen production performance. *Fuel* **2024**, *362*, 130743.

[63] Gu, Y. P.; Li, Y. K.; Feng, H. Q.; Han, Y. A.; Li, Z. J. Built-in electric field induced S-scheme g-C_3N_4 homojunction for efficient photocatalytic hydrogen evolution: Interfacial engineering and morphology control. *Nano Res.* **2024**, *17*, 4961–4970.

[64] Hu, J.; Liu, H. Y.; Sun, C.; Wu, L. X.; Jiao, F. P. Precise defect engineering with ultrathin porous frameworks on g-C_3N_4 for synergetic boosted photocatalytic hydrogen evolution. *Ind. Eng. Chem. Res.* **2024**, *63*, 2665–2675.

[65] Yang, B.; Han, J.; Zhang, Q.; Liao, G. F.; Cheng, W. J.; Ge, G. X.; Liu, J. C.; Yang, X. D.; Wang, R. J.; Jia, X. Carbon defective g-C_3N_4 thin-wall tubes for drastic improvement of photocatalytic H_2 production. *Carbon* **2023**, *202*, 348–357.

[66] Wang, H. T.; Yu, L. L.; Peng, J. H.; Zou, J.; Gong, W. P.; Jiang, J. Z. Experimental and theoretical investigation of sulfur-doped g-C_3N_4 nanosheets/$FeCo_2O_4$ nanorods S-scheme heterojunction for photocatalytic H_2 evolution. *Nano Res.* **2024**, *17*, 8007–8016.

[67] Hou, S. Q.; Gao, X. C.; Wang, S. J.; Yu, X. X.; Liao, J. Y.; Su, D. W. Precise defect engineering on graphitic carbon nitrides for boosted solar H_2 production. *Small* **2024**, *20*, 2302500.

[68] Qin, Y. Y.; Lu, J.; Zhao, X. Y.; Lin, X. Y.; Hao, Y.; Huo, P. W.; Meng, M. J.; Yan, Y. S. Nitrogen defect engineering and π-conjugation structure decorated g-C_3N_4 with highly enhanced visible-light photocatalytic hydrogen evolution and mechanism insight. *Chem. Eng. J.* **2021**, *425*, 131844.

[69] Shan, X.; Ge, G. F.; Zhao, Z. K. Fabrication of tubular g-C_3N_4 with N-defects and extended π-conjugated system for promoted photocatalytic hydrogen production. *ChemCatChem* **2019**, *11*, 1534–1544.

[70] Wang, H. T.; Jiang, J. Z.; Yu, L. L.; Peng, J. H.; Song, Z.; Xiong, Z. G.; Li, N.; Xiang, K.; Zou, J.; Hsu, J. P. et al. Tailoring advanced N-defective and S-doped g-C_3N_4 for photocatalytic H_2 evolution. *Small* **2023**, *19*, 2301116.

[71] Tian, Y. X.; Zeng, D. N.; Shen, T. Z.; Guan, R. F.; Shi, W. Y. One-step synthesis of S-doped C-vacancy g-C_3N_4 with honeycomb porous nanosheets structure for efficient visible-light-driven hydrogen evolution. *Fuel* **2024**, *357*, 129927.

[72] Pu, W. J.; Zhou, Y. Q.; Yang, L. F.; Gong, H. F.; Li, Y. H.; Yang, Q. Y.; Zhang, D. Q. High-efficiency crystalline carbon nitride photocatalysts: Status and perspectives. *Nano Res.* **2024**, *17*, 7840–7863.

[73] Wang, X. C.; Blechert, S.; Antonietti, M. Polymeric graphitic carbon nitride for heterogeneous photocatalysis. *ACS Catal.* **2012**, *2*, 1596–1606.

[74] Cao, S. W.; Li, H.; Tong, T.; Chen, H. C.; Yu, A. C.; Yu, J. G.; Chen, H. M. Single-atom engineering of directional charge transfer channels and active sites for photocatalytic hydrogen evolution. *Adv. Funct. Mater.* **2018**, *28*, 1802169.

[75] Yang, Z. D.; Zhang, Y.; Zhang, H. X.; Zhao, J. H.; Shi, H.; Zhang, M.; Yang, H. Q.; Zheng, Z. F.; Yang, P. J. Nitrogen vacancies in polymeric carbon nitrides promote CO_2 photoreduction. *J. Catal.* **2022**, *409*, 12–23.

[76] Shi, H. N.; Long, S. R.; Hou, J. G.; Ye, L.; Sun, Y. W.; Ni, W. J.; Song, C. S.; Li, K. Y.; Gurzadyan, G. G.; Guo, X. W. Defects promote ultrafast charge separation in graphitic carbon nitride for enhanced visible-light-driven CO_2 reduction activity. *Chem. —Eur. J.* **2019**, *25*, 5028–5035.

[77] Song, X. H.; Zhang, X. Y.; Li, X.; Che, H. N.; Huo, P. W.; Ma, C. C.; Yan, Y. S.; Yang, G. Y. Enhanced light utilization efficiency and fast charge transfer for excellent CO_2 photoreduction activity by constructing defect structures in carbon nitride. *J. Colloid Interface Sci.* **2020**, *578*, 574–583.

[78] Gong, Y. N.; Shao, B. Z.; Mei, J. H.; Yang, W.; Zhong, D. C.; Lu, T. B. Facile synthesis of C_3N_4-supported metal catalysts for efficient CO_2 photoreduction. *Nano Res.* **2022**, *15*, 551–556.

[79] Zhou, Z. R.; Guo, W. Y.; Yang, T. Y.; Zheng, D. D.; Fang, Y. X.; Lin, X. H.; Hou, Y. D.; Zhang, G. G.; Wang, S. B. Defect and nanostructure engineering of polymeric carbon nitride for visible-light-driven CO_2 reduction. *Chin. J. Struct. Chem.* **2024**, *43*, 100245.

[80] Hou, J. H.; Yang, M. Y.; Dou, Q.; Chen, Q.; Wang, X. Z.; Hu, C. G.; Paul, R. Defect engineering in polymeric carbon nitride with accordion structure for efficient photocatalytic CO_2 reduction and H_2 production. *Chem. Eng. J.* **2022**, *450*, 138425.

[81] Liu, Y. Z.; Zhao, L.; Zeng, X. H.; Xiao, F.; Fang, W.; Du, X.; He, X.; Wang, D. H.; Li, W. X.; Chen, H. Efficient photocatalytic reduction of CO_2 by improving adsorption activation and carrier utilization rate through N-vacancy g-C_3N_4 hollow microtubule. *Mater. Today Energy* **2023**, *31*, 101211.

[82] Ma, W.; Wang, N.; Guo, Y.; Yang, L. Q.; Lv, M. F.; Tang, X.; Li, S. T. Enhanced photoreduction CO_2 activity on g-C_3N_4: By synergistic effect of nitrogen defective-enriched and porous structure, and mechanism insights. *Chem. Eng. J.* **2020**, *388*, 124288.

[83] Nor, N. U. M.; Mazalan, E.; Amin, N. A. S. Insights into enhancing photocatalytic reduction of CO_2: Substitutional defect strategy of modified g-C_3N_4 by experimental and theoretical calculation approaches. *J. Alloys Compd.* **2021**, *871*, 159464.

[84] Li, Y. H.; Ren, Z. T.; He, Z. J.; Ouyang, P.; Duan, Y. Y.; Zhang, W. D.; Lv, K. L.; Dong, F. Crystallinity-defect matching relationship of g-C_3N_4: Experimental and theoretical perspectives. *Green Energy Environ.* **2023**, *9*, 623–658.

[85] Zhang, J.; Chen, J. W.; Wan, Y. F.; Liu, H. W.; Chen, W.; Wang, G.; Wang, R. L. Defect engineering in atomic-layered graphitic carbon nitride for greatly extended visible-light photocatalytic hydrogen evolution. *ACS Appl. Mater. Interfaces* **2020**, *12*, 13805–13812.

[86] Gu, Z. Y.; Jin, M. D.; Wang, X.; Zhi, R. T.; Hou, Z. H.; Yang, J.; Hao, H. F.; Zhang, S. Y.; Wang, X. L.; Zhou, E. P. et al. Recent advances in g-C_3N_4-based photocatalysts for NO_x removal. *Catalysts* **2023**, *13*, 192.

[87] Liao, J. Z.; Cui, W.; Li, J. Y.; Sheng, J. P.; Wang, H.; Dong, X. A.; Chen, P.; Jiang, G. M.; Wang, Z. M.; Dong, F. Nitrogen defect structure and NO^+ intermediate promoted photocatalytic NO removal on H_2 treated g-C_3N_4. *Chem. Eng. J.* **2020**, *379*, 122282.

[88] Wang, Z. Y.; Huang, Y.; Chen, M. J.; Shi, X. J.; Zhang, Y. F.; Cao, J. J.; Ho, W.; Lee, S. C. Roles of N-vacancies over porous g-C_3N_4 microtubes during photocatalytic NO_x removal. *ACS Appl. Mater. Interfaces* **2019**, *11*, 10651–10662.

[89] Duan, Y. Y.; Li, X. F.; Lv, K. L.; Zhao, L.; Liu, Y. Flower-like g-C_3N_4 assembly from holy nanosheets with nitrogen vacancies for efficient NO abatement. *Appl. Surf. Sci.* **2019**, *492*, 166–176.

[90] Huang, X. Y.; Li, X. Y.; Chen, A. K.; Gu, H. F.; Li, S. Y.; Hou, T. L.; Zhu, S. W.; Yu, S.; Song, Y.; Zhang, J. T. Electronic structure engineering of single atomic sites by plasmon-induced hot electrons for highly efficient and selective photocatalysis. *Nano Res.* **2024**, *17*, 6960–6967.

[91] Li, Y. H.; Ho, W.; Lv, K. L.; Zhu, B. C.; Lee, S. C. Carbon vacancy-induced enhancement of the visible light-driven photocatalytic oxidation of NO over g-C_3N_4 nanosheets. *Appl. Surf. Sci.* **2018**, *430*, 380–389.

[92] Dong, G. H.; Jacobs, D. L.; Zang, L.; Wang, C. Y. Carbon vacancy regulated photoreduction of NO to N_2 over ultrathin g-C_3N_4 nanosheets. *Appl. Catal. B: Environ.* **2017**, *218*, 515–524.

[93] Wang, H.; He, W. J.; Dong, X. A.; Wang, H. Q.; Dong, F. *In situ* FT-IR investigation on the reaction mechanism of visible light photocatalytic NO oxidation with defective g-C_3N_4. *Sci. Bull.* **2018**, *63*, 117–125.

[94] Shen, H. D.; Yang, M. M.; Hao, L. D.; Wang, J. R.; Strunk, J.; Sun, Z. Y. Photocatalytic nitrogen reduction to ammonia: Insights into the role of defect engineering in photocatalysts. *Nano Res.* **2022**, *15*, 2773–2809.

[95] Nguyen, D. L. T.; Tekalgne, M. A.; Nguyen, T. H. C.; Dinh, M. T. N.; Sana, S. S.; Grace, A. N.; Shokouhimehr, M.; Vo, D. V. N.; Cheng, C. K.; Nguyen, C. C. et al. Recent development of high-performance photocatalysts for N_2 fixation: A review. *J. Environ. Chem. Eng.* **2021**, *9*, 104997.

[96] Gong, Y. Y.; Xu, Z. D.; Wu, J.; Zhong, J. B.; Ma, D. M. Enhanced photocatalytic hydrogen production performance of g-C_3N_4 with rich carbon vacancies. *Appl. Surf. Sci.* **2024**, *657*, 159790.

[97] Zhang, L.; Hou, S. Q.; Wang, T. Y.; Liu, S. X.; Gao, X. C.; Wang, C. Y.; Wang, G. X. Recent advances in application of graphitic carbon nitride-based catalysts for photocatalytic nitrogen fixation. *Small* **2022**, *18*, 2202252.

[98] Li, L. J.; Zhang, P.; Li, N.; Reyila, T.; Yu, Y. C.; Su, X. P.; Peng, C.; Han, L. J. Application of g-C_3N_4-based photocatalysts for N_2 photofixation. *J. Environ. Chem. Eng.* **2024**, *12*, 112142.

[99] Zhang, Y. N.; Li, S.; Sun, C.; Cao, X. R.; Wang, X.; Yao, J. N. Defective g-C_3N_4 supported Ru_3 single-cluster catalyst for ammonia synthesis through parallel reaction pathways. *Nano Res.* **2023**, *16*, 3580–3587.

[100] Li, Y. S.; Ti, M. R.; Zhao, D. X.; Zhang, Y.; Wu, L.; He, Y. J. Facile synthesis of nitrogen-vacancy pothole-rich few-layer g-C_3N_4 for photocatalytic nitrogen fixation into nitrate and ammonia. *J. Alloys Compd.* **2021**, *870*, 159298.

[101] Wang, W. K.; Zhou, H. J.; Liu, Y. Y.; Zhang, S. B.; Zhang, Y. X.; Wang, G. Z.; Zhang, H. M.; Zhao, H. J. Formation of B-N-C coordination to stabilize the exposed active nitrogen atoms in g-C_3N_4

for dramatically enhanced photocatalytic ammonia synthesis performance. *Small* **2020**, *16*, 1906880.

[102] Xue, Y. J.; Guo, Y. C.; Liang. Z. Q.; Cui, H. Z.; Tian, J. Porous g-C_3N_4 with nitrogen defects and cyano groups for excellent photocatalytic nitrogen fixation without co-catalysts. *J. Colloid. Interface Sci.* **2019**, *556*, 206–213.

[103] Sun, C.; Chen, Z. Q.; Cui, J.; Li, K.; Qu, H. X.; Xie, H. F.; Zhong, Q. Site-exposed Ti_3C_2 MXene anchored in N-defect g-C_3N_4 heterostructure nanosheets for efficient photocatalytic N_2 fixation. *Catal. Sci. Technol.* **2021**, *11*, 1027–1038.

[104] Song, J.; Dai, J.; Zhang, P.; Liu, Y. T.; Yu, J. Y.; Ding, B. g-C_3N_4 encapsulated ZrO_2 nanofibrous membrane decorated with CdS quantum dots: A hierarchically structured, self-supported electrocatalyst toward synergistic NH_3 synthesis. *Nano Res.* **2021**, *14*, 1479–1487.

[105] Ye, X. L.; Shi, S. T.; Zeng, Y. B.; Ding, M. Y.; Wu, Z. K. Carbon defective carbon nitride with large specific surface area by hot oxygen etching for promoting photocatalytic performance. *Colloid Surf. A* **2022**, *632*, 127732.

[106] Cao, S. H.; Chen, H.; Jiang, F.; Wang, X. Nitrogen photofixation by ultrathin amine-functionalized graphitic carbon nitride nanosheets as a gaseous product from thermal polymerization of urea. *Appl. Catal. B: Environ.* **2018**, *224*, 222–229.

[107] Dong, G. H.; Ho, W.; Wang, C. Y. Selective photocatalytic N_2 fixation dependent on g-C_3N_4 induced by nitrogen vacancies. *J. Mater. Chem. A* **2015**, *3*, 23435–23441.

[108] Xue, Y. J.; Ma, C. Q.; Yang, Q. F.; Wang, X. Y.; An, S. N.; Zhang, X. L.; Tian, J. Construction of g-C_3N_4 with three coordinated nitrogen (N_{3C}) vacancies for excellent photocatalytic activities of N_2 fixation and H_2O_2 production. *Chem. Eng. J.* **2023**, *457*, 141146.

[109] Zhang, Y.; Di. J.; Ding, P. H.; Zhao, J. Z.; Gu, K. Z.; Chen, X. L.; Yan, C.; Yin, S.; Xia, J. X.; Li, H. M. Ultrathin g-C_3N_4 with enriched surface carbon vacancies enables highly efficient photocatalytic nitrogen fixation. *J. Colloid Interface Sci.* **2019**, *553*, 530–539.

[110] Kong, Y.; Lv, C. D.; Zhang, C. M.; Chen, G. Cyano group modified g-C_3N_4: Molten salt method achievement and promoted photocatalytic nitrogen fixation activity. *Appl. Surf. Sci.* **2020**, *515*, 146009.

[111] Xu, J.; Wang, Z. P.; Zhu, Y. F. Highly efficient visible photocatalytic disinfection and degradation performances of microtubular nanoporous g-C_3N_4 via hierarchical construction and defects engineering. *J Mater. Sci. Technol.* **2020**, *49*, 133–143.

[112] Zhen, X. L.; Fan, C. Z.; Tang, L.; Luo, J.; Zhong, L. R.; Gao, Y. Y.; Zhang, M. J.; Zheng, J. F. Advancing charge carriers separation and transformation by nitrogen self-doped hollow nanotubes g-C_3N_4 for enhancing photocatalytic degradation of organic pollutants. *Chemosphere* **2023**, *312*, 137145.

[113] Chen, J. Q.; Lin, W. T.; Xie, L. Y.; Huang, J. H.; Wang, W. J. Templated fabrication of graphitic carbon nitride with ordered mesoporous nanostructures for high-efficient photocatalytic bacterial inactivation under visible light irradiation. *J. Nanomater.* **2019**, *2019*, 3242136.

[114] Wang, J.; Dou, M. M.; Wang, X. Y.; Gao, B. R.; Zhuang, T.; Ma, Z. K. Synergetic mechanism of defective g-C_3N_4 activated persulfate on removal of antibiotics and resistant bacteria: ROSs transformation, electron transfer and noncovalent interaction. *Chemosphere* **2022**, *294*, 133741.

[115] Zhong, K. Q.; Xie, D. H.; Liu, Y. J.; Guo, P. C.; Sheng, G. P.; Modulation of ultrathin nanosheet structure and nitrogen defects in graphitic carbon nitride for efficient photocatalytic bacterial inactivation. *Water Res. X* **2023**, *20*, 100193.

[116] Liu, H. P.; Ma, S. L.; Shao, L.; Liu, H. T.; Gao, Q. C.; Li, B. J.; Fu, H. C.; Fu, S.; Ye, H. G.; Zhao, F. Y. et al. Defective engineering in graphitic carbon nitride nanosheet for efficient photocatalytic pathogenic bacteria disinfection. *Appl. Catal. B: Environ.* **2020**, *261*, 118201.

[117] Dahlan, N. A. N.; Putri, L, K.; Er, C. C.; Ng, B. J.; Ooi, C. W.; Tan, L. L.; Chai, S. P. Effective low-powered photocatalytic disinfection via synchronous introduction of oxygen dopants and carbon defects in carbon nitride. *ACS Appl. Mater. Interfaces* **2023**, *15*, 53371–53381.

[118] Huang, X.; Song, M.; Zhang, J.; Zhang, J. J.; Liu, W.; Zhang, C.; Zhang, W.; Wang, D. L. Investigation of MXenes as oxygen reduction electrocatalyst for selective H_2O_2 generation. *Nano Res.* **2022**, *15*, 3927–3932.

[119] Pi, L.; Cai, J. H.; Xiong, L. L.; Cui, J. X.; Hua, H. L.; Tang, D. D.; Mao, X. H. Generation of H_2O_2 by on-site activation of molecular dioxygen for environmental remediation applications: A review. *Chem. Eng. J.* **2020**, *389*, 123420.

[120] He, Q.; Viengkeo, B.; Zhao, X.; Qin, Z. Y.; Zhang, J.; Yu, X. H.; Hu, Y. P.; Huang, W.; Li, Y. G. Multiscale structural engineering of carbon nitride for enhanced photocatalytic H_2O_2 production. *Nano Res.* **2023**, *16*, 4524–4530.

[121] Fattahimoghaddam, H.; Mahvelati-Shamsabadi, T.; Lee, B. K. Enhancement in photocatalytic H_2O_2 production over g-C_3N_4 nanostructures: a collaborative approach of nitrogen deficiency and supramolecular precursors. *ACS Sustain. Chem. Eng.* **2021**, *9*, 4520–4530.

[122] Luo, J.; Liu, Y. N.; Fan, C. Z.; Tang, L.; Yang, S. J.; Liu, M. L.; Wang, M. E.; Feng, C. Y.; Ouyang, X. L.; Wang, L. L. et al. Direct attack and indirect transfer mechanisms dominated by reactive oxygen species for photocatalytic H_2O_2 production on g-C_3N_4 possessing nitrogen vacancies. *ACS Catal.* **2021**, *11*, 11440–11450.

[123] Zhang, H.; Jia, L. H.; Wu, P.; Xu, R. J.; He, J.; Jiang, W. Improved H_2O_2 photogeneration by KOH-doped g-C_3N_4 under visible light irradiation due to synergistic effect of N defects and K modification. *Appl. Surf. Sci.* **2020**, *527*, 146584.

[124] Li, R. J.; Deng, Q. F.; Chen, A. L.; Zhong, Y. J.; Yang, R. Synthesis of double defects in g-C_3N_4 to enhance the H_2O_2 production by dual-electron O_2 reduction. *ChemSusChem* **2023**, *16*, e202300763.

[125] Shi, L.; Yang, L. Q.; Zhou, W.; Liu, Y. Y.; Yin, L. S.; Hai, X.; Song, H.; Ye, J. H. Photoassisted construction of holey defective g-C_3N_4 photocatalysts for efficient visible-light-driven H_2O_2 production. *Small* **2018**, *14*, 1703142.

[126] Li, J. N.; Huang, J. H.; Zeng, G. M.; Zhang, C. Y.; Yu, H. B.; Wan, Q. F.; Yi, K. X.; Zhang, W.; Pang, H. L.; Liu, S. et al. Efficient photosynthesis of H_2O_2 via two-electron oxygen reduction reaction by defective g-C_3N_4 with terminal cyano groups and nitrogen vacancies. *Chem. Eng. J.* **2023**, *463*, 142512.

[127] Li, R. J.; Zheng, M.; Zhou, X.; Zhang, D.; Shi, Y.; Li, C. X.; Yang, M. Carbon vacancies in porous g-C_3N_4 nanosheets induced robust H_2O_2 production for highly efficient photocatalysis-self-Fenton system for metronidazole degradation. *Chem. Eng. J.* **2023**, *464*, 142584.